**Forschungszentrum Karlsruhe**
Technik und Umwelt
**Wissenschaftliche Berichte**
FZKA 5912

# A Model for Radiative Heat Transfer in Mixtures of a Hot Solid or Molten Material with Water and Steam

**L. Väth**

**Institut für Neutronenphysik und Reaktortechnik**
**Projekt Nukleare Sicherheitsforschung**

**Mai 1997**

**Forschungszentrum Karlsruhe**
**Technik und Umwelt**
**Wissenschaftliche Berichte**
FZKA 5912

# A Model for Radiative Heat Transfer in Mixtures of a Hot Solid or Molten Material with Water and Steam

L. Väth
Institut für Neutronenphysik und Reaktortechnik
Projekt Nukleare Sicherheitsforschung

Forschungszentrum Karlsruhe GmbH, Karlsruhe
1997

Forschungszentrum Karlsruhe GmbH
Postfach 3640, 76021 Karlsruhe

ISSN 0947-8620

Abstract:

A model has been devised for describing the radiative heat transfer in mixtures of a hot radiant material with water and steam, to be used, e. g., in the framework of a multiphase, multicomponent flow simulation. The main features of the model are:

1. The radiative heat transfer is modelled for a homogeneous mixture of one continuous material with droplets/bubbles of the other two, of the kind normally assumed for the material distribution in one cell of a bigger calculational problem. Neither the heat transfer over the cell boundaries nor the finite dimensions of the cell are taken into account.
2. The geometry of the mixture (radiant material continuous or discontinuous, droplet/bubble diameters and number densities) is taken into account.
3. The optical properties of water and water vapour are modelled as functions of the temperature of the radiant and, in the case of water vapour, also of the absorbing material.
4. The model distinguishes between heat transfer to the surface of the water (leading to evaporation) and into the bulk of the water (pure heating).

Care has been taken to approximate the real physical phenomena in a very simple way in order to maintain calculational efficiency, because the model is to be applied in the framework of a much bigger code. A few examples demonstrating the effect of the model on calculations with the multiphase, multicomponent code IVA-KA are presented.

Ein Modell der Wärmeübertragung durch Strahlung für Mischungen eines heißen festen oder flüssigen Materials mit Wasser und Dampf

Zusammenfassung:

Ein Modell zur Beschreibung der Wärmeübertragung durch Strahlung in Mischungen eines heißen strahlenden Materials mit Wasser und Dampf wurde entwickelt; es kann beispielsweise bei der Simulation von Mehrphasen-Mehrkomponenten-Strömungen zum Einsatz kommen. Die wesentlichen Eigenschaften des Modells sind:

1. Die Wärmeübertragung durch Strahlung wird für eine homogene Mischung eines kontinuierlichen Materials mit Tropfen bzw. Blasen der anderen zwei modelliert, d. h. in einer Geometrie, wie sie üblicherweise zur Beschreibung der Verhältnisse innerhalb einer Zelle eines umfassenderen Rechenproblems verwendet wird. Weder die Wärmeübertragung über die Zellgrenzen hinaus noch die endlichen Dimensionen der Zelle werden berücksichtigt.
2. Die Geometrie der Mischung (kontinuierlicher oder diskontinuierlicher Zustand des Strahlers, Tropfen-/Blasendurchmesser und -zahldichte) wird berücksichtigt.
3. Die optischen Eigenschaften von Wasser und Dampf werden als Funktion der Temperatur des Strahlers und, bei Wasserdampf, auch des Absorbers modelliert.
4. Das Modell unterscheidet zwischen Wärmedeposition auf der Wasseroberfläche (die zu Verdampfung führt) und im Wasservolumen (reine Aufheizung).

Die in der Realität stattfindenden physikalischen Prozesse werden aus Gründen der Recheneffizienz mit sehr einfachen Modellen angenähert, da das Modell für einen wesentlich umfangreicheren Code bestimmt ist. An einigen Beispielen wird der Einfluss des Modells auf Rechnungen mit dem Mehrphasen-Mehrkomponenten-Code IVA-KA demonstriert.

**Content:**


| | | |
|---|---|---|
| 1. | Introduction | 1 |
| 2. | Heat transfer from the radiant material to water | 2 |
| 2.1. | Geometries to be treated | 2 |
| 2.2. | Absorption of radiation along a given distance | 4 |
| 2.3. | Mean distance between melt surfaces for the different flow regimes | 8 |
| 2.4. | Net absorption of radiation in water | 13 |
| 2.5. | Relation of volume and surface absorption | 14 |
| 3. | Heat transfer from the radiant material to water vapour | 16 |
| 3.1. | Absorption and emission of radiation in water vapour | 16 |
| 3.2. | Net absorption of radiation in water vapour | 21 |
| 3.3. | Absorption in a mixture of water and water vapour | 21 |
| 4. | Examples of calculations with the new model | 24 |
| 4.1. | Parametric studies | 25 |
| 4.2. | Simple examples with 2x2 cells | 33 |
| 4.3. | Simulation of experiment FARO L-08 | 39 |
| 5. | Conclusions | 43 |
| Table of symbols | | 44 |
| References | | 45 |

## 1. INTRODUCTION

The treatment of radiative heat transfer forms one important part of any model attempting to describe the interaction of molten material with water, e. g., in codes for evaluating the premixing phase preceding possible vapour explosions. The reason is that, at temperatures above a few hundred degrees C, heat transfer by radiation becomes nonnegligible in relation to that by convection, and its influence gets decisive at around $2000^0$C.

The computer code IVA-KA /1/ is currently being developed at FZK for investigating the premixing phase of possible vapour explosions in thermal reactors and the explosion proper; it can also be used quite generally for describing three phase, three component mixing phenomena. This code has been derived from an older version, IVA3 /2/, which was developed in 1990 and 1991 by N. I. Kolev at FZK. One of the main features distinguishing the new version from the old one is the new model for heat transfer by radiation, which replaced an older, somewhat simplistic one.

When devising a model for one of the many physical phenomena to be taken into account in a code like IVA-KA, one must keep in mind that radiative heat transfer forms an important but nevertheless very small part of the constitutive relations, which themselves are only one part of the total modelling. It is therefore necessary to keep the calculational effort for the phenomenon within very stringent limits, in order to maintain acceptable running times for the code and also a certain equilibrium with the other models. Thus, instead of modelling physical details, a very simple model is devised, taking care that the main effects are described.

The modelling will be presented in the next two sections; the introduction to section 2 contains also those details of the modelling employed in IVA-KA that define the geometry for the radiative heat transfer model. Some examples of calculations with the new model and a comparison with the older one contained in IVA3 are presented in section 4. The conclusions follow in section 5.

## 2. HEAT TRANSFER FROM RADIANT MATERIAL TO WATER

### 2.1. Geometries to be treated

Details on the purpose and layout of the code IVA3 can be found in ref. /2/. It is sufficient for this presentation to state that among the three material fields modelled by the code the first one contains a mixture of water vapour and air, the second one water in the liquid state, and the third one the radiant material. This section deals thus with the radiative heat transfer from field 3 to field 2.

The geometry to be represented in a calculation is subdivided into a number of cells, as is normal for this kind of code. Time dependent volume fractions of the three material fields (and their state variables, velocities etc.) are calculated for each cell. A flow regime is assigned to each cell, depending on the volume fraction of the fields and in part on their physical state. Fig. 1 (from ref. /3/) shows a schematic representation of the flow regimes realized in IVA3 (including some that are of no interest for the studies foreseen in FZK-INR or not realized at present, i. e. the numbers 6, 8, 10, 11, 12 and 13). The flow regimes of interest for this section are those containing water and melt: 2 and 3 (without field 1), and 5, 21 and 23 (containing field 1 in addition to fields 2 and 3).

It is quite simple, without changing the given data management in IVA3, to add new terms for heat transfer within one cell, since such terms are provided for already. A major difficulty arises, however, when radiative heat transfer across the cell boundaries is to be modelled, since all heat transfer to adjacent cells is coupled to a convective mass transfer in IVA3. Treating this problem would require the introduction of additional terms in the source term of the entropy equation. This has not been foreseen at present, but might become necessary in the future, if the modelling of intra-cell radiative heat transfer alone proves to be too restrictive.

Three assumptions are made in the following:

1. The radiation emitted by the melt is assumed to have the spectral distribution of black body radiation.

2. The radiant material is opaque, i. e. any radiation reaching its surface is totally absorbed. This assumption holds for the molten materials treated by the code (steel, oxides of uranium, plutonium...).

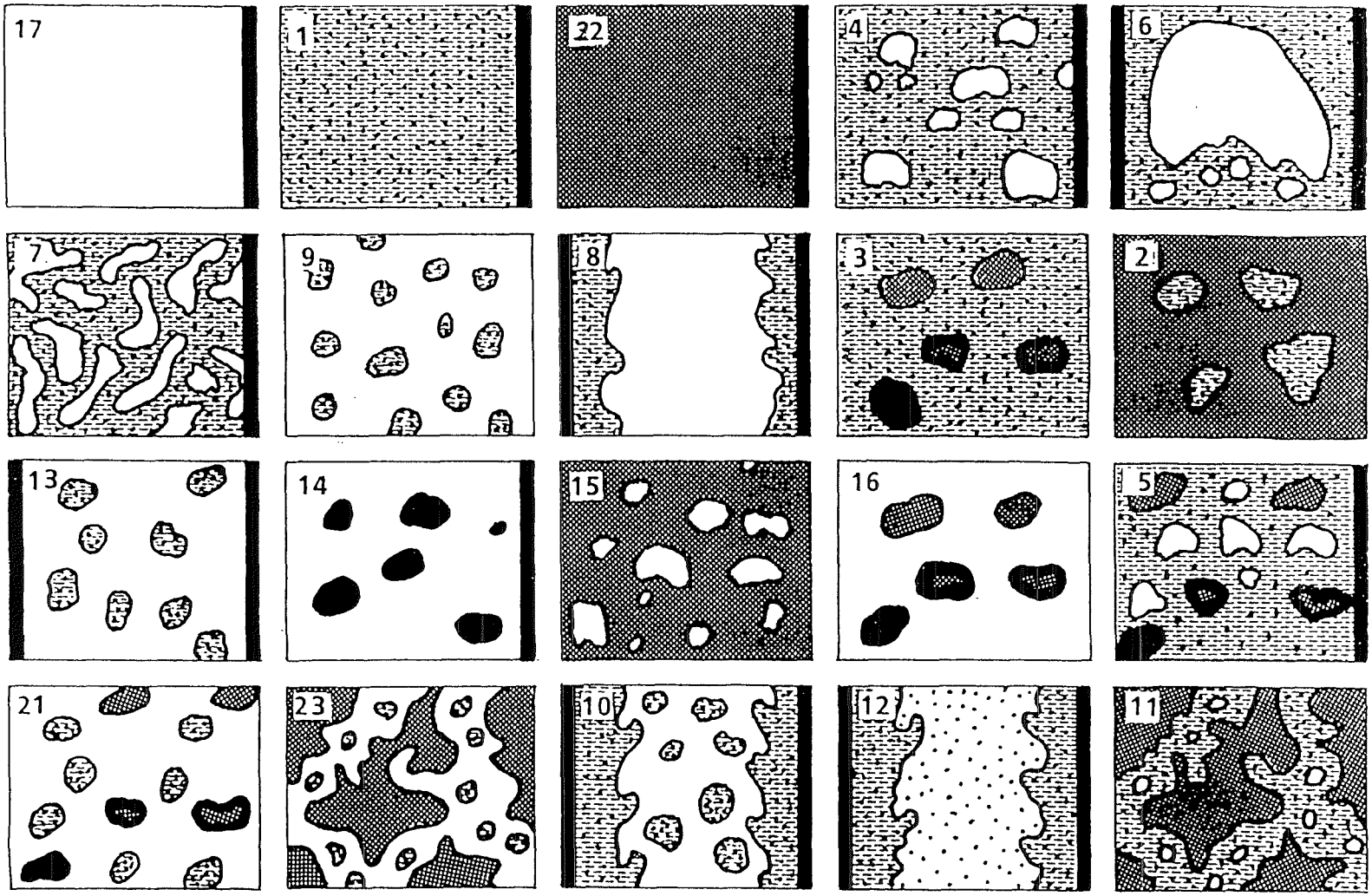


Fig. 1: Flow regimes employed in IVA-KA.

3. The geometry given by the flow regime in one particular cell can be extended to infinity for the purpose of calculating the radiative heat transfer. This is normally a good approximation, since the cell dimensions tend to be of the order of at least several centimeters, and bubble/droplet/particle sizes are typically one or a few millimeters only.

The third assumption leads to an overprediction of the intra-cell radiative heat transfer, which can somewhat compensate for neglecting the extra-cell radiative heat transfer, especially since the transfer of liquid and gas out of the cell can be expected to be enhanced by the additional heating.

## 2.2. Absorption of radiation along a given distance

The absorption in water depends on the wavelength of the incident radiation as shown in fig. 2 /4/ for a temperature of 20°C and a pressure of 1 bar. The absorption coefficient increases from negligible values to practically total opacity at wavelengths between 1 and 3 $\mu$m. Black body radiation has its maximum intensity at 1.5 $\mu$m for a temperature of 2000 K (see fig. 3); typical melt temperatures range from 1000 to 3000 K. It follows, that a partial absorption of the radiation in water must be modelled, depending on the temperature of the radiant material and the thickness of the water layer.

The exact way for arriving at the absorption coefficient for the total radiation emitted is to take explicitely into account the dependence on the wavelength and integrate numerically over the whole spectrum, for the temperature of the radiant material in each cell. In addition, this must be done for the different distances the radiation can travel before being absorbed on the surface of a neighbouring melt droplet, and the results are to be averaged. This procedure is obviously far too time consuming, and has to be simplified decisively.

First, the spectrum of distances between melt surfaces is replaced by an average value, and it is assumed, that the average of the absorption along the different distances can be replaced by the absorption along the average distance. One is then left with approximating the absorptivity $A_w$ as a function of the mean distance S and the temperature $T_3$ of the radiant material (material field 3).

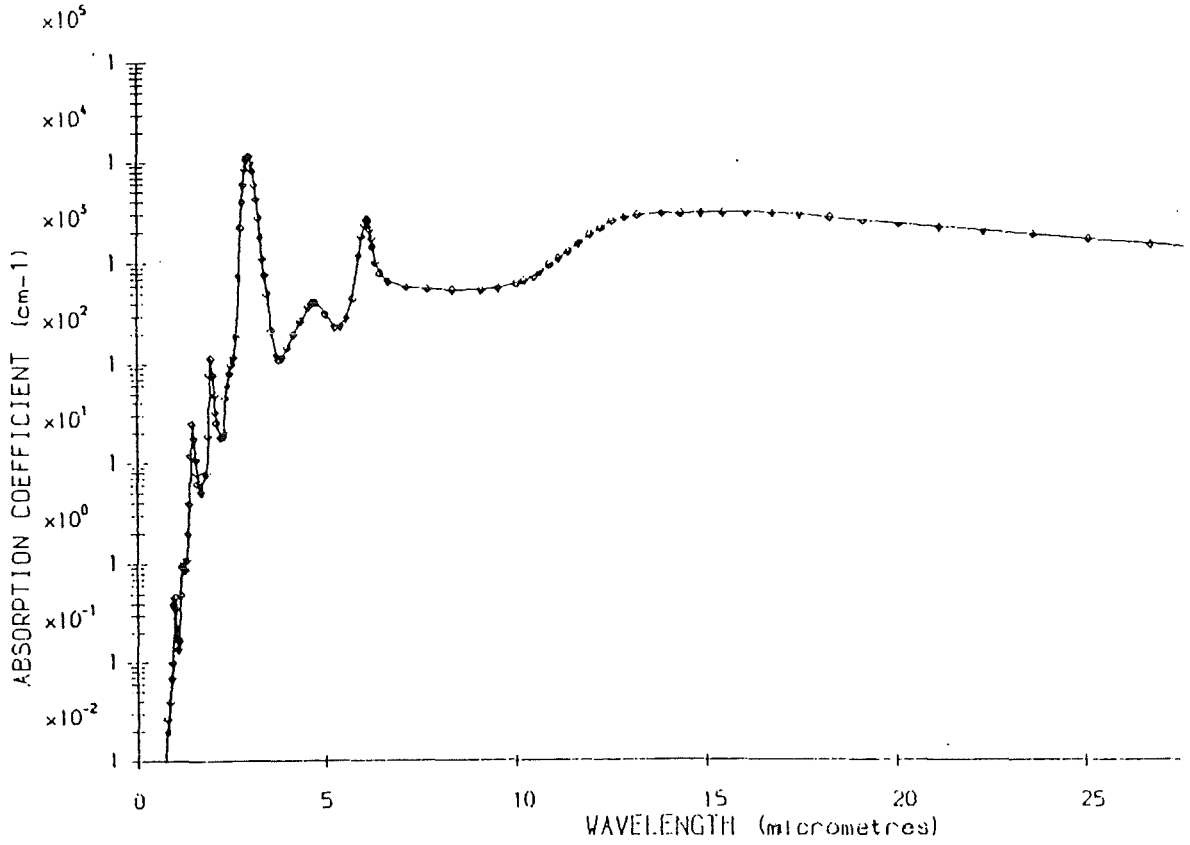


Fig. 2: Absorption coefficient as a function of the wavelength for water at 20°C and 1 bar /4/.

Fletcher /4/ presents a table of numerical results for the fractions of energy absorbed in water layers with thicknesses between 1 and 30 mm and temperatures of the black body of 1000, 2500 and 3500 K. It is reproduced below as table I. An asymptotic behaviour is observed for distances exceeding 15 mm. The values of Fletcher's table are employed in IVA-KA in the following way (which is a further simplification):

First a suitable function is employed for representing the columns of table I. Such a function is

$$A_w(S) = a \ln(S^b + 1) \qquad (1)$$

This function yields the correct value for $S=0$: $A_w(S=0)=0$. The two parameters a and b must be derived from table I; they are calculated in such a way that the values for $S = 1$ mm, $A_1$, and for $S = 30$ mm, $A_{30}$, are correctly represented. The parameters a and b result from this condition and eq. (1) as

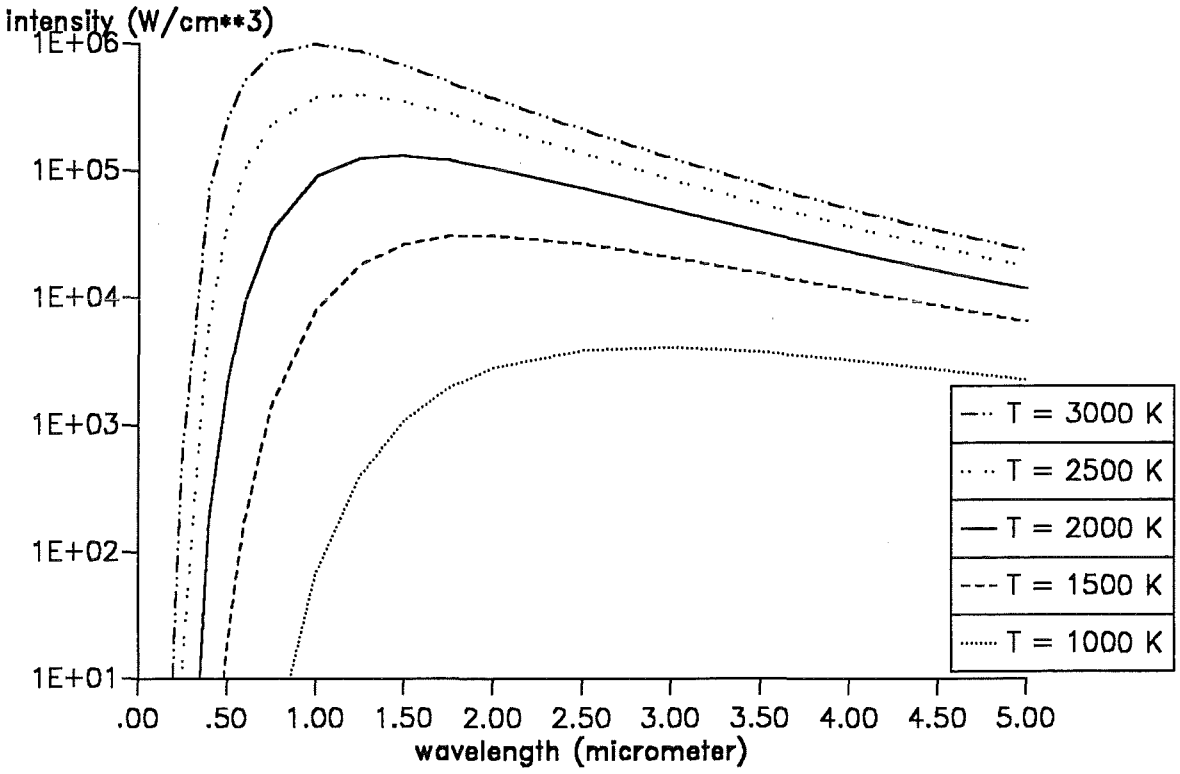


Fig. 3: Intensity of black body radiation as a function of the wavelength according to Stefan-Boltzmann's law, for different temperatures.

| S (mm) | $T_3$ = 1000 K | $T_3$ = 2500 K | $T_3$ = 3500 K |
|---|---|---|---|
| 1 | 0.967 | 0.599 | 0.343 |
| 5 | 1.000 | 0.707 | 0.472 |
| 10 | 1.000 | 0.756 | 0.526 |
| 15 | 1.000 | 0.786 | 0.560 |
| 20 | 1.000 | 0.806 | 0.585 |
| 25 | 1.000 | 0.822 | 0.604 |
| 30 | 1.000 | 0.834 | 0.620 |

**Table I:** Fraction of energy $A_w(S, T_3)$ absorbed by a water layer of thickness S from the radiation of a black body at temperature $T_3$ /4/.

$$a = A_1/\ln 2$$
$$b = \ln\left[2^{A_{30}/A_1} - 1\right]/\ln 30 \qquad (2)$$

They are evaluated from table I for the three different temperatures. This results in the following three functions $A_{10}(S)$, $A_{25}(S)$ and $A_{35}(S)$ describing the absorptivity of water for the temperatures 1000, 2500 and 3500 K:

$$A_{10}(S) = 1.395086 \ln\left[S^{.01374877} + 1\right] \quad (\text{for} T = 1000K)$$
$$A_{25}(S) = .8641743 \ln\left[S^{.1427472} + 1\right] \quad (\text{for} T = 2500K) \qquad (3)$$
$$A_{35}(S) = .4948444 \ln\left[S^{.2694667} + 1\right] \quad (\text{for} T = 3500K)$$

These three equations are used instead of table I for calculating the fraction of energy absorbed in water in the subprogramme OPAWAT (OPAcity of WATer) in IVA-KA. They are shown in fig. 4 together with the values of table I.

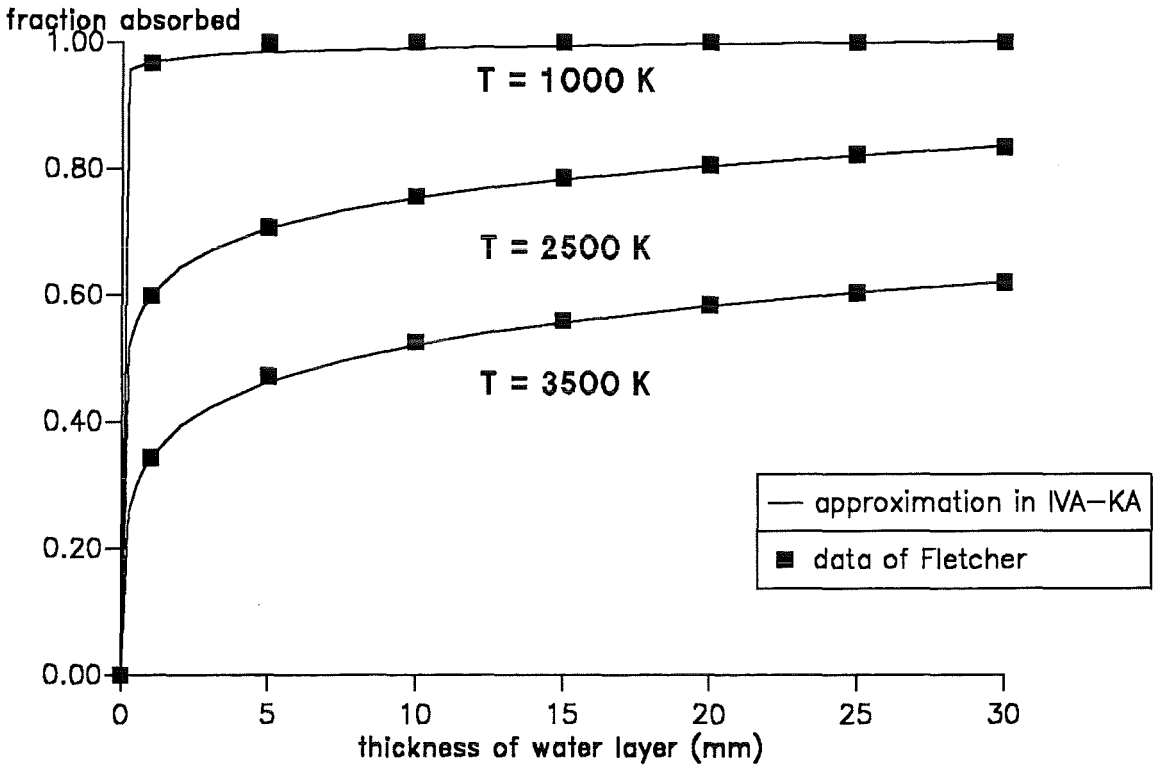


Fig. 4: Absorption in water at different temperatures according to table I and as approximated in IVA-KA, as a function of the thickness of the water layer.

The first step of the calculation in OPAWAT for given values of S and $T_3$ consists thus of evaluating $A_{10}(S)$, $A_{25}(S)$ and $A_{35}(S)$. One must then interpolate for the temperature $T_3$. This is done with a second order polynomial

$$A_w(S, T_3) = c + dT + eT^2$$

The parameters c, d and e are calculated from the conditions $A_w(S,1000) = A_{10}(S)$, $A_w(S,2500) = A_{25}(S)$, and $A_w(S,3500) = A_{35}(S)$. The result is the following equation for the temperature interpolation:

$$\begin{aligned} A_w(S, T_3) = {} & \frac{A_{10}(S)}{15}(35 + 4T'(-6 + T')) \\ & + \frac{A_{25}(S)}{3}(-7 + T'(9 - 2T')) \\ & + \frac{A_{35}(S)}{5}(5 + T'(-7 + 2T')) \\ \text{with } T' = {} & T_3/1000 \end{aligned} \tag{4}$$

This numerical procedure represents the values of Fletcher's table excellently (see fig. 4) and gives reasonable results even outside the range of table I. Some additional restrictions have to be imposed, however, when extrapolating:

1. $T_3 \leq 5000$ K; if $T_3 > 5000$ K, use 5000 K. The second order polynomial in $T_3$ may yield values increasing with temperature beyond 5000 K instead of the physically reasonable decreasing values. It should be kept in mind that extrapolating so far beyond the range of table I is not reasonable anyway and will not be required in the applications intended.

2. $0 \leq A_w(S, T_3) \leq 1$; $A_w$ as calculated from eq. (4) may exceed 1 for temperatures below 1000 K due to the properties of the polynomial being employed for the temperature dependence.

3. $A_w(S, T_3) = 1$ for $T_3 \leq 1000$ K and $S \geq 30$ mm. The extrapolation into this domain has been found to yield values slightly below 1, which are thus corrected.

## 2.3. Mean distance between melt surfaces for the different flow regimes

The mean distance that has to be traversed by radiation emitted from a point on the surface of the radiant material until it strikes another particle of field 3 depends on the flow regime (fig. 1) and the volume fraction of field 3. Among the

regimes of interest in this section (2, 3, 5, 21 and 23), number 2 is the only one with a continuous field 3. Field 2 is idealized as spherical droplets of equal size with diameter $D_2$ in this case; this is consistent with other heat transfer models in IVA-KA. The mean distance is then (for the geometry see fig. 6 with $D_2$ replacing $D_c$ and $D_3 = 0$)

$$\bar{S}(\text{regime 2}) = \int_0^{\pi/2} S(\theta) \sin\theta \, d\theta = D_2 \int_0^{\pi/2} \cos\theta \, \sin\theta \, d\theta = \frac{1}{2} D_2$$

Field 3 is modelled as dispersed droplets for all other regimes (including regime 23, with relatively little volume surrounding the droplets). In this case field 3 is idealized as spherical droplets of equal size with diameter $D_3$, which is again consistent with the other heat transfer models in IVA-KA. The following approximations are used for estimating the mean distance of the surfaces for the radiation:

1. Each droplet is surrounded by its share of field 1 + field 2 volume, which forms a spherical shell with outer diameter $D_c$ (fig. 5). Droplet and surrounding shell together will be called "mini-cell" in the following, since the concept recalls the Wigner-Seitz-cell used in nuclear reactor physics /5/ ("mini"-cell in order to avoid confusion with the IVA-KA mesh cells).

2. As a first step, the mean distance a ray emitted from the surface of the droplet travels till reaching the surface of its mini-cell is calculated. It is called $S_i$.

3. After leaving the mini-cell in which it has originated, the ray enters another mini-cell (of identical geometry). The probability of traversing this mini-cell without absorption by the melt droplet and the mean distance $S_t$ for traversing are determined.

4. The mean distance $S_f$ through the cell for a ray entering a mini-cell and striking the droplet is also calculated.

5. In the end, the probabilities for a ray of traversing 0, 1, 2 etc. adjacent mini-cells before being reabsorbed by a field 3 droplet are determined together with the associated mean distances. Weighting all distances with their probabilities and summarizing results in the overall mean distance.

The geometry for finding $S_i$ is shown in fig. 5, which is a cut through the mini-cell in the plane of the radiation emitted. The real situation is three-dimensional but

symmetric around the vertical axis, and can thus be reduced to fig. 5. The diameter of the mini-cell is related to the volume fraction of field 3, $\alpha_3$, and the diameter of the melt droplet by

$$D_c = \frac{D_3}{\sqrt[3]{\alpha_3}} \tag{5}$$

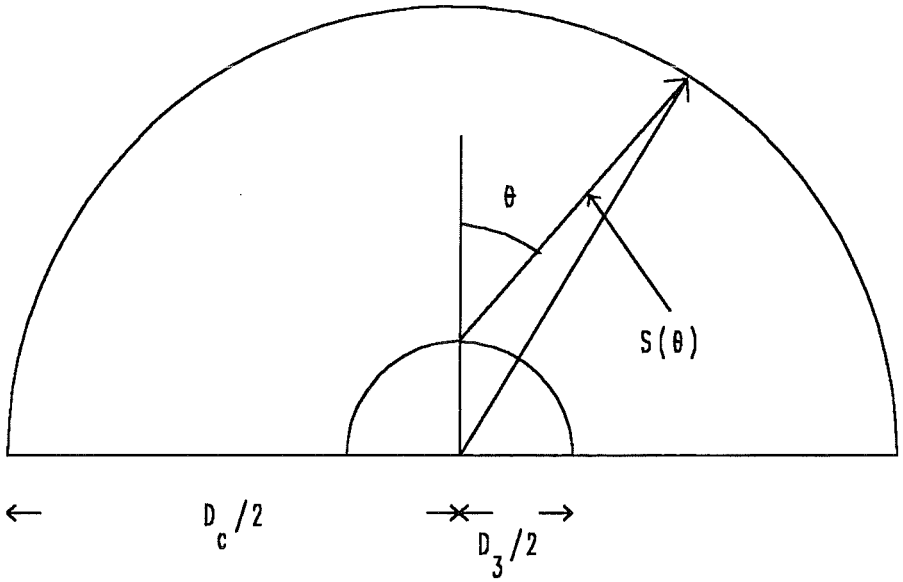


Fig. 5: Geometry for calculating mean distances: Emission of radiation from a cell.

$S_i$ is given by

$$S_i = \int_0^{\pi/2} S(\theta) \sin\theta \, d\theta$$

When $S(\theta)$ is expressed as a function of $D_c$ and $D_3$, it follows

$$S_i = \frac{D_c - D_3}{4} + \frac{D_3}{8}\left(\frac{D_c^2}{D_3^2} - 1\right) \ln \frac{D_c + D_3}{D_c - D_3}$$

or, with the help of eq. (5):

$$S_i = \frac{D_c}{4}\left[1 - \sqrt[3]{\alpha_3} + \frac{1}{2}\left(\frac{1}{\sqrt[3]{\alpha_3}} - \sqrt[3]{\alpha_3}\right) \ln \frac{1 + \sqrt[3]{\alpha_3}}{1 - \sqrt[3]{\alpha_3}}\right] \tag{6}$$

The limits for $\alpha_3$ approaching 0 resp. 1 are, as expected

$$S_i(\alpha_3 << 1) \simeq \frac{D_c}{2}\left[1 - \frac{\sqrt[3]{\alpha_3}}{2}\right] \simeq \frac{D_c}{2}$$

$$S_i(\alpha_3 \simeq 1) \simeq \frac{D_c}{4}(1 - \sqrt[3]{\alpha_3})\left[1 + \ln\frac{2}{1 - \sqrt[3]{\alpha_3}}\right] \simeq 0$$

Fig. 6 shows the geometric conditions for radiation entering the mini-cell from the outside. radiation entering within the limiting angle $\theta_{lim}$ will be absorbed by the droplet, the rest will pass through the mini-cell to the next one. The probability P for absorption is calculated with the assumption of an isotropic distribution of the radiation entering the mini-cell. With

$$\sin\theta_{lim} = \frac{D_3}{D_c}$$

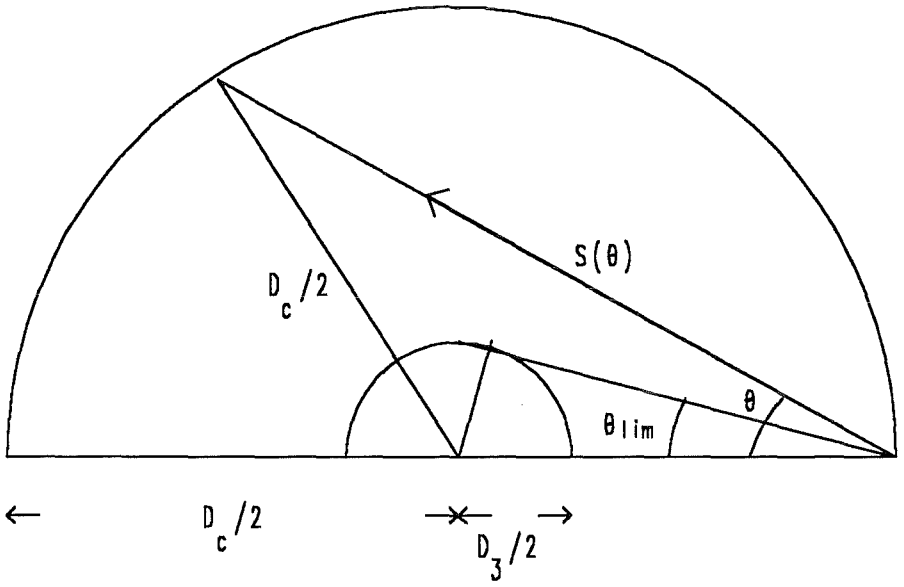


Fig. 6: Geometry for calculating mean distances: radiation entering a cell from the outside.

it results as

$$P = \int_0^{\theta_{lim}} \sin\theta\, d\theta = 1 - \sqrt{1 - \sqrt[3]{\alpha_3}^2} \qquad (7)$$

The mean distance through the mini-cell for the radiation traversing it is

$$S_t = \frac{1}{1-P} \int_{\theta_{lim}}^{\pi/2} S(\theta) \sin\theta \, d\theta$$

Since

$$S(\theta) = D_c \cos(\theta)$$

$S_t$ results as

$$S_t = \frac{D_c}{2} \sqrt{1 - \sqrt[3]{\alpha_3^2}} \tag{8}$$

The mean distance through the mini-cell for the radiation being absorbed can be calculated in the same way as $S_t$, but the resulting formula is somewhat lengthy. However, since the problem resembles the one for the outgoing radiation, since $S_f$ forms only a small contribution to the total distance, and since a number of approximations are involved anyway, it suffices to postulate

$$S_f = S_i \tag{9}$$

One can now derive the average distance $\overline{S}$ for the radiation from emission to absorption in field 3. The fraction emitted in one mini-cell and absorbed in the next one is P, and the average distance till absorption for this part of the radiation is $S_i + S_f$; its contribution to the average distance is thus

$$P \times (S_i + S_f) = P \times 2S_i$$

The radiation traversing one mini-cell before being reabsorbed contributes

$$(1-P)P \times (2S_i + S_t)$$

and radiation traversing two mini-cells before absorption

$$(1-P)^2 P \times (2S_i + 2S_t)$$

and so forth, resulting in the mean distance for all radiation:

$$\begin{aligned}\bar{S} &= P \times 2S_i + (1-P)P \times (2S_i + S_t) + (1-P)^2 P \times (2S_i + 2S_t) + \ldots \\ &= 2S_i + \frac{(1-P)}{P} \times S_t\end{aligned} \tag{10}$$

2.4. Net absorption of radiation in water

Knowing the mean distance for the radiation from emission to reabsorption in the melt, one can now calculate its absorption in water along that distance. First one has to take into account the fraction of gas in the volume. Since the effect of the gas is accounted for separately, an effective distance $S_w$ through water alone must be applied. With $\alpha_1$ and $\alpha_2$ denoting the volume fractions occupied by gas and water, respectively, $S_w$ results as

$$S_w = \bar{S} \frac{\alpha_2}{\alpha_1 + \alpha_2} \tag{11}$$

The energy (per unit mixture volume) emitted by the radiant material is

$$Q = O \sigma \varepsilon_3 T_3^4 \tag{12}$$

where $\varepsilon_3$ is the emissivity of the melt (presently .7 is used in IVA-KA), $T_3$ is its temperature, $\sigma$ is the Stefan-Boltzmann constant ($5.669710^{-8} W/(m^2K^4)$), and O is the surface of the melt per unit mixture volume. O depends on the geometry of the flow regime and is given in table II below (flow regimes of importance for the next chapter are included; $D_1$ is the diameter of the gas bubbles).

| Flow regime | Surface |
|---|---|
| 2 | $6\alpha_2 / D_2$ |
| 3,5,16,21,23 | $6\alpha_3 / D_3$ |
| 15 | $6\alpha_1 / D_1$ |

**Table II:** Melt surfaces for the different geometries.

The net energy absorbed by the water, $dQ_w$ results from eq. (12), taking into account the radiation reemitted, as

$$dQ_w = A_w(S_w, T_3)\, O\, \sigma\, \varepsilon_3\, T_3^4 \left[ 1 - \left( \frac{T_2}{T_3} \right)^4 \right] \qquad (13)$$

2.5. Relation of volume and surface absorption

A distinction is made in this model between the radiative energy absorbed on the surface or in the bulk of the water. The energy absorbed in the bulk serves to raise the bulk temperature of the water whereas absorption on the surface causes primarily its evaporation. One must therefore calculate, in addition to the energy absorbed, its distribution between bulk and surface of the water.

It has been observed in section 2.2 already, that the absorption in water increases from negligible values to a high value at wavelengths between 1 and 3 $\mu$m and then remains practically constant (see fig. 2). As a very simple approximation to these conditions, it is assumed, that radiation between 1 and 3 $\mu$m undergoes volume absorption because of the lower absorptivity for these wavelengths. The radiation with wavelengths exceeding 3 $\mu$m is assumed to be absorbed on the surface. The thickness of the water layer is not taken into account. The resulting distribution function depends only on the temperature of the radiant material under these assumptions. Stefan-Boltzmann's law governs the spectral distribution of black body radiation and gives for the energy radiated in the interval from 1 to 3 $\mu$m

$$E_{vol}(T_3) = \int_{\lambda = 1\ \mu m}^{\lambda = 3\ \mu m} \left[ \lambda^5 \left( \exp\left( \frac{hc}{\lambda k T_3} \right) - 1 \right) \right]^{-1} d\lambda$$

($\lambda$ wavelength, h Planck's constant, c velocity of light, k Boltzmann constant). The energy radiated above 3 $\mu$m is, similarly

$$E_{surf}(T_3) = \int_{\lambda = 3\ \mu m}^{\infty} \left[ \lambda^5 \left( \exp\left( \frac{hc}{\lambda k T_3} \right) - 1 \right) \right]^{-1} d\lambda$$

The fraction of the absorbed energy deposited in the surface is then

$$F_{surf}(T_3) = \frac{E_{surf}(T_3)}{E_{surf}(T_3) + E_{vol}(T_3)}$$

$F_{surf}(T_3)$ was calculated numerically for a number of temperatures and then approximated with the following function:

$$\tilde{F}_{surf}(T_3) = \min\left(1., \frac{x^2}{x^2 - .4611115x + .8366274}\right) \qquad (14)$$
$$x = 1000/T_3$$

$F_{surf}$ and $\tilde{F}_{surf}$ are shown in fig. 7. Note that the approximation reaches the value 1 at $x = 1.814$ ($T_3 = 551$ K). The model thus assumes that radiation emitted by a melt at temperatures below 551 K is absorbed in the surface of water only.

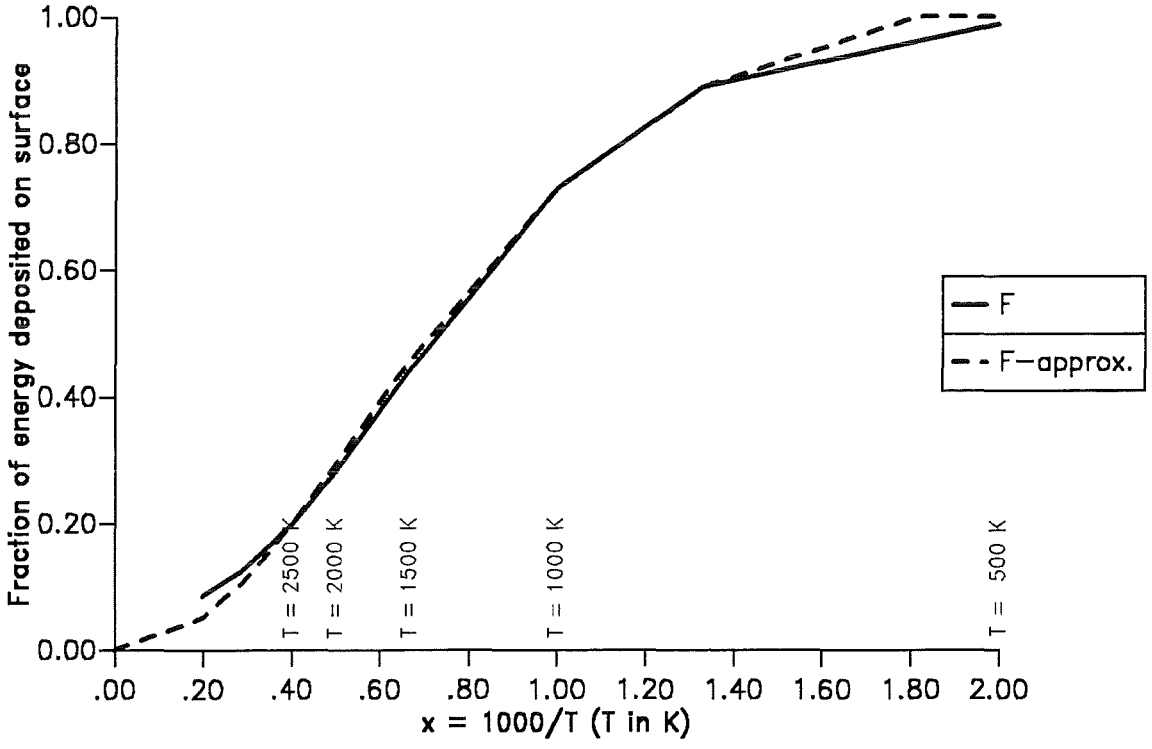


Fig. 7: Fraction of radiative energy absorbed at the surface of water; calculation from the spectral distribution of wavelengths above 1 $\mu$m and numerical approximation used in IVA-KA.

## 3. HEAT TRANSFER FROM THE RADIANT MATERIAL TO WATER VAPOUR

Water vapour absorbes radiation from the same spectral region as water, i. e. at wavelengths above 1 $\mu$m, but the energy dependence of its absorptivity differs decidedly from that of water. Therefore, and also because its temperature may differ from that of the water in the same cell, it must be treated separately.

Many publications on the calculation of absorption by water vapour deal also with the simultaneous absorption by carbon dioxide. Of course carbon dioxide is not needed in the model presented here, because applications related to the burning of fossile fuels are not planned at present. It should be mentioned that a simple inclusion of carbon dioxide is not possible with this model, because the gas is about as efficient an absorber as water vapour and has its absorption bands in the same energy region. Therefore the interaction of both cannot be treated with something like a single correction factor, but would have to be modelled in more detail.

The flow regimes containing the gaseous phase (field 1) together with field 3 and of interest for applications in FZK are: 15, 16 (fields 1 and 3 only), and 5, 21 and 23 (all three fields). The modelling of the heat transfer to water vapour will be presented in the first two subsections below; the third part of the section addresses the problem of combining the transfer from field 3 to both field 1 and field 2.

The three basic assumptions made for radiative heat transfer to water will also be employed here, namely: Black body radiation, opaque radiant material, and extension of the geometry of the flow regime to infinity (see the introduction to section 2).

### 3.1. Absorption and emission of radiation in water vapour

Water vapour may be at a much higher temperature than water, and thus its emissivity becomes important and must be taken into account, if the net absorption of radiative energy is to be calculated with some degree of accuracy. The absorptivity - and, similarly, the emissivity - shows a number of energy bands due to the different vibrational and rotational states of the molecule and their interaction. They are subject to different broadening mechanisms (Doppler-effect, pressure) and are therefore very sensitive to the physical state of the gas, as demonstrated in fig. 8.

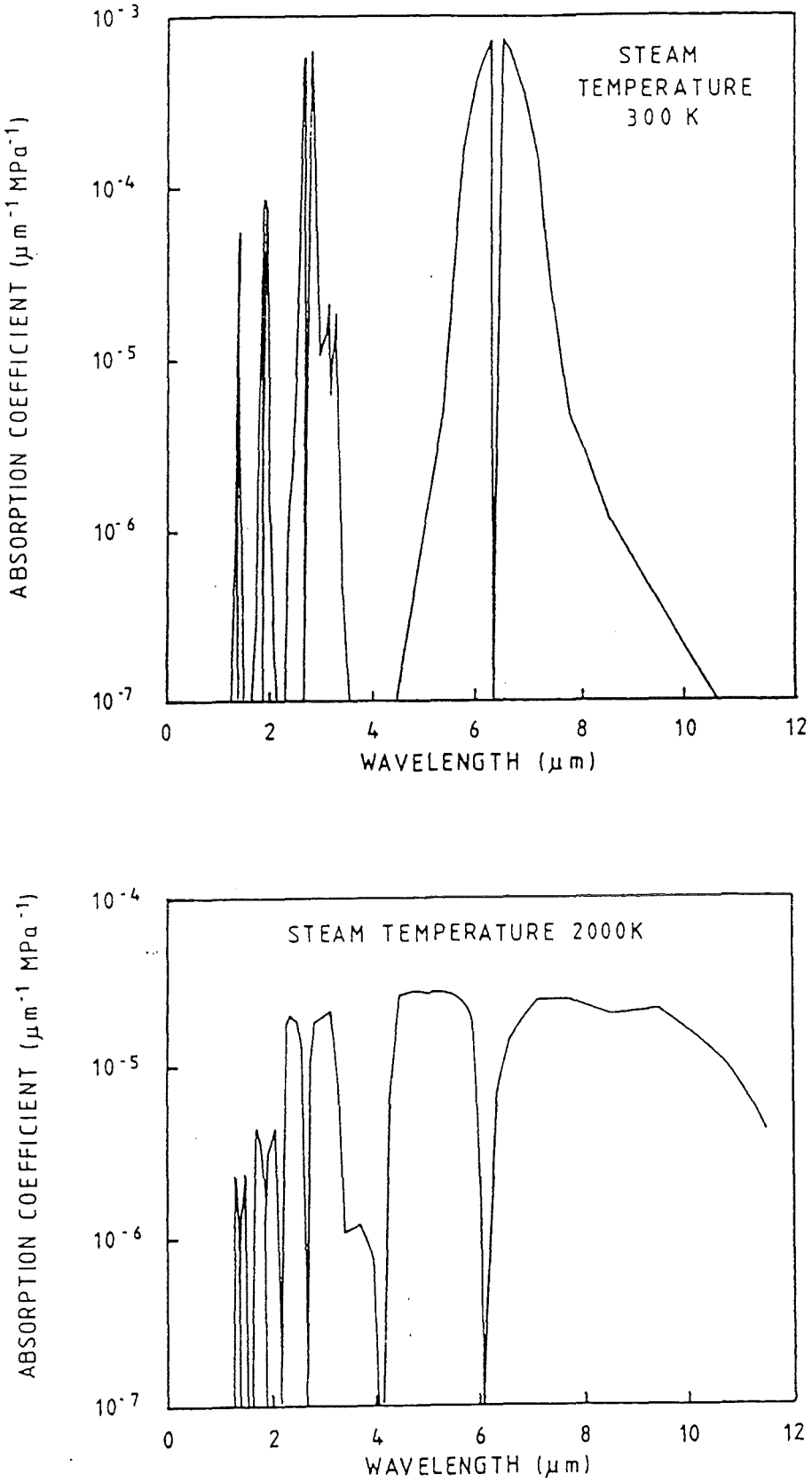


Fig. 8: Absorption coefficient of water vapour at 300 K and 2000 K as a function of the wavelength /6/.

Water vapour plays a role in many industrial processes, and therefore quite a lot of effort has been invested already into representing its radiative properties for modelling purposes /6/, /7/, /8/, /9/. The results of these investigations - mostly graphs - were transformed into simplified functions for use in IVA-KA.

The main parameters governing the emissivity and absorptivity of water vapour are its temperature $T_1$ and the product of its partial pressure $p_v$ and the thickness of the layer traversed by the radiation, S. This second parameter, $p_vS$, will be called y in the following.

Ten values of the emissivity of water vapour $\varepsilon_v$ pertaining to two values of $T_1$ (800 and 2800 K) and five values of y (200, 3050, 20000, 152400 and 1524000 Pa•m) were chosen among the results of experiments and calculations presented in the papers of Docherty /8/ and Steward and Kocaefe /9/. Experimental results are used whenever possible. The values chosen are shown in fig. 9. They serve as the basic grid for the inter- and extrapolation.

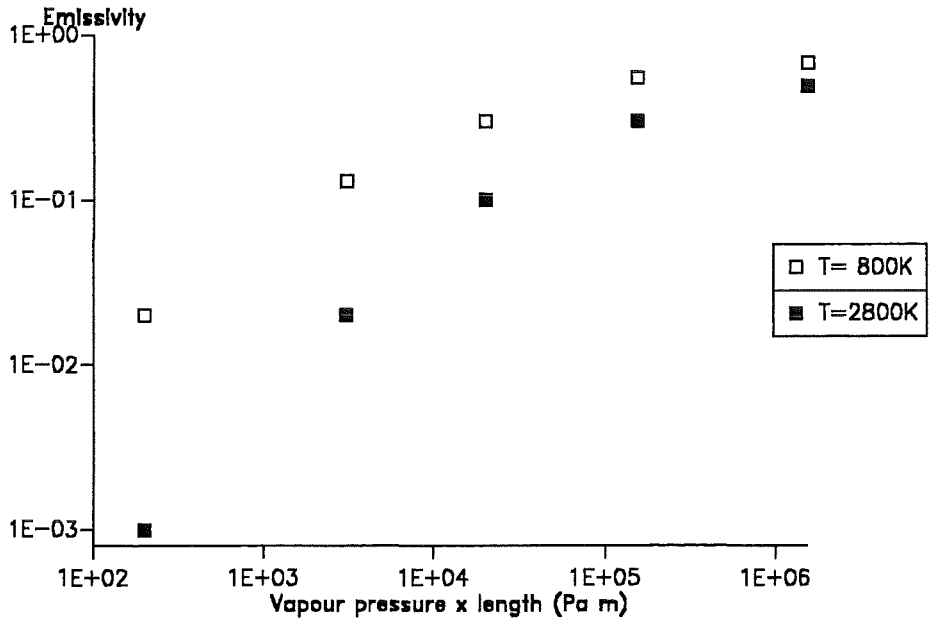


Fig. 9: Values used for interpolating the water vapour emissivity.

The inter- and extrapolation is performed in the following way: The interpolation with respect to the temperature is performed first. A linear interpolation is used for temperatures below 2800 K, including the extrapolation to values below 800 K. The general function is

$$\varepsilon_v(y, T_1) = \varepsilon_v(y,800) + (\varepsilon_v(y,2800) - \varepsilon_v(y,800)) \frac{T_1 - 800}{2000} \tag{15}$$

Eq. (15) is evaluated numerically using the values of the basic grid shown in fig. 9. This results in the following 5 functions, that are actually programmed:

$$\begin{aligned}
\varepsilon_v(y = 200, T_1 \leq 2800K) &= .0276 - 0.95\,10^{-5} T_1 \\
\varepsilon_v(y = 3050, T_1 \leq 2800K) &= .174 - 0.55\,10^{-4} T_1 \\
\varepsilon_v(y = 20000, T_1 \leq 2800K) &= .38 - 1.00\,10^{-4} T_1 \\
\varepsilon_v(y = 152400, T_1 \leq 2800K) &= .65 - 1.25\,10^{-4} T_1 \\
\varepsilon_v(y = 1524000, T_1 \leq 2800K) &= .756 - 0.95\,10^{-4} T_1
\end{aligned} \tag{16}$$

When extrapolating to temperatures above 2800 K, a function should be utilized that smoothly approaches zero, because even for high temperatures the spectrum of black body radiation contains always a small fraction of longer wave radiation in the range of the absorption bands. An exponential extrapolation of the form

$$\varepsilon_v(y, T_1) = a(y)\, e^{b(y)T_1} \tag{17}$$

is able to model this behaviour. If the parameters a and b are chosen in such a way that the value and the gradient of $\varepsilon_v$ at 2800 K are reproduced, the following general extrapolation function results from eq. (17):

$$\varepsilon_v(y, T_1) = \varepsilon_v(y,2800) \exp\left( - \frac{\varepsilon_v(y,800) - \varepsilon_v(y,2800)}{\varepsilon_v(y,2800)} \frac{T_1 - 2800}{2000} \right) \tag{18}$$

This function is also evaluated numerically for the basic grid, resulting in the following 5 functions used in the programme:

$$\begin{aligned}
\varepsilon_v(y = 200, T_1 > 2800K) &= .001 \exp(-9.5\,10^{-3}(T_1 - 2800)) \\
\varepsilon_v(y = 3050, T_1 > 2800K) &= .02 \exp(-2.75\,10^{-3}(T_1 - 2800)) \\
\varepsilon_v(y = 20000, T_1 > 2800K) &= .1 \exp(-10^{-3}(T_1 - 2800)) \\
\varepsilon_v(y = 152400, T_1 > 2800K) &= .3 \exp(-\frac{25}{6}\,10^{-4}(T_1 - 2800)) \\
\varepsilon_v(y = 1524000, T_1 > 2800K) &= .49 \exp(-\frac{95}{49}\,10^{-4}(T_1 - 2800))
\end{aligned} \tag{19}$$

The second interpolation in the y-direction, including the extrapolation to values exceeding 1524000 Pa•m, is performed with linear functions linking the neighbouring points in fig. 9 (linear in the double logarithmic representation employed in fig. 9). The interpolation functions are thus

$$\ln(\varepsilon_v(y, T_1)) = c(T_1) + d(T_1) \ln y$$

When $c(T_1)$ and $d(T_1)$ are determined from the two values $y_1$ and $y_2$ in fig. 9 that bracket the given value of y (or the two highest values in the case of an extrapolation), and from $\varepsilon_1$ and $\varepsilon_2$, the corresponding values of the emissivity obtained from eq. (16) or (19), the following inter-(extra-)polation formula results:

$$\ln(\varepsilon_v(y, T_1)) = \frac{\ln(\varepsilon_1(T_1)) \times \ln\frac{y}{y_2} + \ln(\varepsilon_2(T_1)) \times \ln\frac{y_1}{y}}{\ln\frac{y_1}{y_2}} \qquad (20)$$

The extrapolation to values below 200 Pa•m is performed with a linear function, noting that the emissivity equals 0 at $y = 0$. If the final result is outside the physically meaningful interval $0 \leq \varepsilon_v \leq 1$, it is set to 0 resp. 1.

The absorptivity $A_v$ of water vapour depends, in addition to $T_1$ and y, on the wavelengths of the radiation and thus on the temperature of the source, $T_3$. It is calculated from the emissivity in a manner recommended by Hottel and Sarofim /7/:

$$A_v(y, T_1, T_3) = (T_1/T_3)^{.45} \varepsilon_v(yT_3/T_1, T_3) \qquad (21)$$

The calculations described so far in this subsection are programmed in the subroutine OPAVAP (OPAcity of VAPour) in IVA-KA. The input to the routine consists of the temperatures $T_1$ and $T_3$ and the product y of the partial vapour pressure and the effective distance through the vapour; the output are the absorptivity and the emissivity. The effective distance $S_v$ is calculated in the same way as in the case of water (see eq. (11)), so that $S_w + S_v = \bar{S}$:

$$S_v = \bar{S} \frac{\alpha_1}{\alpha_1 + \alpha_2} \qquad (22)$$

$\bar{S}$ depends on the flow regime as in section 2: It is identical with the $\bar{S}$ calculated in section 2 for the regimes 5, 21 and 23, is calculated in the same way as for

those regimes in the case of regime 16, and is, for regime 15, analogous to regime 2:

$$\bar{S}(\text{regime 15}) = \frac{1}{2} D_1$$

3.2. Net absorption of radiation in water vapour

The net energy absorbed by the water vapour, $dQ_v$ results in the same way as eq. (13), taking into account the radiation emitted by the vapour:

$$dQ_v = O\,\sigma\,\varepsilon_3\,T_3^4\left[A_v(y, T_1, T_3) - \varepsilon_v(y, T_1)\left(\frac{T_1}{T_3}\right)^4\right] \qquad (23)$$

with the radiating surface of field 3, O, given in table II for the flow regimes of interest. The following condition has to be imposed on $A_v$ in order to ensure the correct direction of heat transfer (from the hotter to the colder material) even when extrapolating outside the range of the measurements shown in fig. 9:

$$A_v(y, T_1, T_3) \geq \varepsilon_v(y, T_1)\left(\frac{T_1}{T_3}\right)^4 \quad \text{for} \quad T_1 \leq T_3$$

$$A_v(y, T_1, T_3) \leq \varepsilon_v(y, T_1)\left(\frac{T_1}{T_3}\right)^4 \quad \text{for} \quad T_1 \geq T_3$$

3.3. Absorption in a mixture of water and water vapour

Water and water vapour are present together in the flow regimes 5, 21 and 23. The heat transfer to both materials cannot be modelled by simply using eq.'s (13) and (23) independently, since the materials absorb from the same range of wavelengths, and thus the presence of one material tends to diminish the effect of the other. Instead a correction is deduced from the considerations following below.

Using the definition of the energy Q emitted by the radiant material according to eq. (12), one can rewrite eq.'s (13) and (23) as (the arguments are omitted for simplicity):

$$dQ_w = Q\,A_w\left(1 - \frac{T_2^4}{T_3^4}\right) = a_w\,Q \qquad (24)$$

$$dQ_v = Q\left(A_v - \varepsilon_v \frac{T_1^4}{T_3^4}\right) = a_v Q \tag{25}$$

If one assumes an exponential law to describe the absorption along the distance s, the differential equation for the absorption in one material only (e. g. water vapour) is

$$\frac{dQ(s)}{ds} = -a_v' Q(s) \tag{26}$$

with the unknown parameter $a_v'$. The solution is the postulated exponential function

$$Q(s) = Qe^{-a_v' s} \tag{27}$$

and $a_v'$ can be found from the conditions at $s = \bar{S}$:

$$Qe^{-a_v' \bar{S}} = Q(1 - a_v)$$
$$a_v' = -\frac{\ln(1 - a_v)}{\bar{S}}$$

When this result is inserted into eq. (27), Q(s) results as

$$Q(s) = Q\,(1 - a_v)^{s/\bar{S}}$$

When two materials are present, eq. (26) is changed to

$$\frac{dQ(s)}{ds} = -(a_v' + a_w')\,Q(s)$$

and it is supposed that $a_v'$ and $a_w'$ remain the same as for one material only. The solution of this equation is

$$Q(s) = Q\,(1 - a_v)^{s/\bar{S}}\,(1 - a_w)^{s/\bar{S}}$$

One arrives at the total energy absorbed over the distance $\bar{S}$ by evaluating this equation for $s = \bar{S}$ and subtracting the result from the energy radiated, Q. This is the total energy the radiant material transfers to water and water vapour, $dQ_{eff}$.

$$dQ_{eff} = Q(a_v + a_w - a_v a_w) \tag{28}$$

The energies transferred to the individual material fields, $dQ_{w,eff}$ and $dQ_{v,eff}$, must, of course, add up to $dQ_{eff}$,

$$dQ_{v,eff} + dQ_{w,eff} = dQ_{eff}$$

and their ratio is postulated to be the same as that of $dQ_v$ and $dQ_w$:

$$\frac{dQ_{v,eff}}{dQ_{w,eff}} = \frac{dQ_v}{dQ_w} = \frac{a_v}{a_w}$$

The solution of these two equations is

$$\begin{aligned} dQ_{w,eff} &= dQ_w\left(1 - \frac{a_v a_w}{a_v + a_w}\right) \\ dQ_{v,eff} &= dQ_v\left(1 - \frac{a_v a_w}{a_v + a_w}\right) \end{aligned} \tag{29}$$

One can easily verify that $dQ_{eff}$, $dQ_{v,eff}$ and $dQ_{w,eff}$ fulfill the following conditions, as required by physical considerations:

$$\begin{aligned} dQ_{eff} &\leq dQ_v + dQ_w \\ dQ_{eff} &\leq Q \\ dQ_{eff} &\simeq dQ_v + dQ_w \quad \text{for small } dQ_v \text{ and } dQ_w \\ dQ_{v,eff} &= dQ_v \quad \text{if } dQ_w = 0, \text{ and vice versa.} \end{aligned}$$

## 4. EXAMPLES OF CALCULATIONS WITH THE NEW MODEL

This section is started with a presentation of the absorption of radiation in mixtures of water and steam, as calculated by the model. The model has been run outside the framework of any code for this study, for different ambient pressures, volume fractions of all three fields, and diameters of field 3 particles/droplets.

Since the model is part of the code IVA-KA, as has been mentioned in the introduction, some calculations with this code will be presented in the rest of the section. They are compared not only with calculations without radiative heat transfer to water, to vapour or to both, but also with the old model for radiative heat transfer contained in IVA3 (which has been reinserted in IVA-KA for this purpose). The old model can be characterized as follows:

1. The radiative heat transfer takes place only inside one calculational cell, as in the new model.
2. The optical properties of water and its vapour are not modelled.
3. The absorption in water depends only in a very rudimentary way on the geometry pertaining to the different flow regimes, and not at all on the temperature of the radiant material.
4. Direct heat transfer to water vapour is not taken into account.
5. The phenomenon is not treated consistently for all flow regimes.

Five different calculations are compared for each of the cases to be examined in sections 4.2 and 4.3. The model for convective heat transfer contained in IVA-KA is the same in all of these calculations. The model for radiative heat transfer has been changed in the following way:

1. The standard (new) model;
2. no radiative heat transfer to vapour ("no vapour" in the figures);
3. no radiative heat transfer to water ("no water" in the figures);
4. no radiative heat transfer at all;
5. the IVA3 (old) model.

Very simple examples are presented in section 4.2; they are useful for examining the basic effects of the model changes and their dependence on individual constellations. A more realistic example follows, involving the simulation of an experiment, though with a somewhat too coarse geometry. It should be stressed that all effects depend very much on the actual problem, and that the cases pre-

sented do not cover all possible situations. When treating distinctly different cases, the results may turn out to differ considerably from those presented below.

## 4.1. Parametric studies

This section consists mainly of a number of figures showing the fraction of the energy radiated, which is absorbed by a mixture of water and steam. The following parameters are kept constant in any one figure: The temperatures of the three fields, the steam pressure, and the diameter of the field 3 particles/droplets. The steam temperature is 2000 K in all cases but one, where steam at the saturation temperature has been investigated. The water temperature is always the saturation temperature for the pressure cited.

The first set of figures, fig.s 10-12, concerns a steam pressure of .1 MPa (water temperature 373 K) and a particle diameter of .005 m, a rather large value that characterizes transient conditions during fragmentation. The three figures are for field 3 temperatures of 2500, 3000 and 3500 K. The absorption is plotted as a function of the field 3 volume fraction, for different values of the parameter G, which is defined as

$$G = \frac{\alpha_1}{\alpha_1 + \alpha_2}$$

G is thus the volume fraction of steam (void fraction) in the steam/water mixture excluding field 3. The full lines represent the total absorption, whereas the dotted ones show the fraction absorbed in water. Evidently the absorption in steam plays a role only for very small field 3 volume fractions in these cases. The bigger absorption for smaller field 3 temperatures, that is to be expected from the wavelength dependence of the absorptivities, becomes obvious when comparing the three figures. One should however keep in mind, that this relates only to the fraction of energy absorbed; the absolute value of the energy absorbed is dominated by the energy radiated, which grows according to eq. (12).

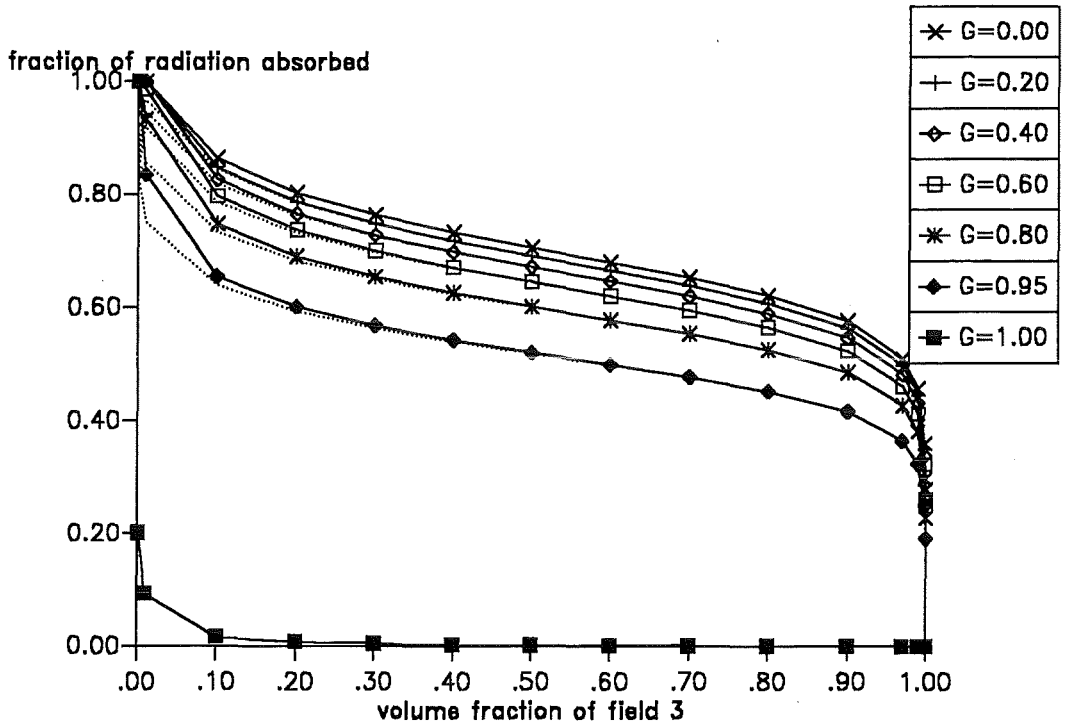


Fig. 10: Absorption of radiation. Temperature of the radiant material 2500 K, steam pressure .1 MPa, steam temperature 2000 K, particle diameter .005 m (full lines: total absorption; dotted lines: absorption in water).

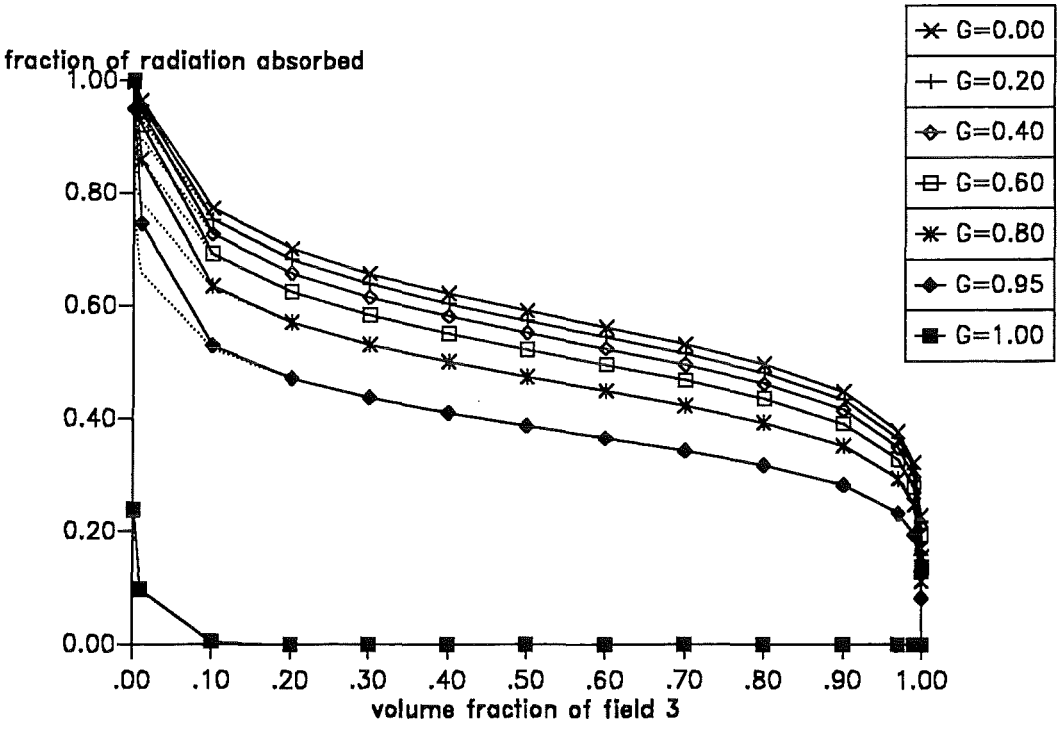


Fig. 11: As fig. 10 for a temperature of the radiant material of 3000 K.

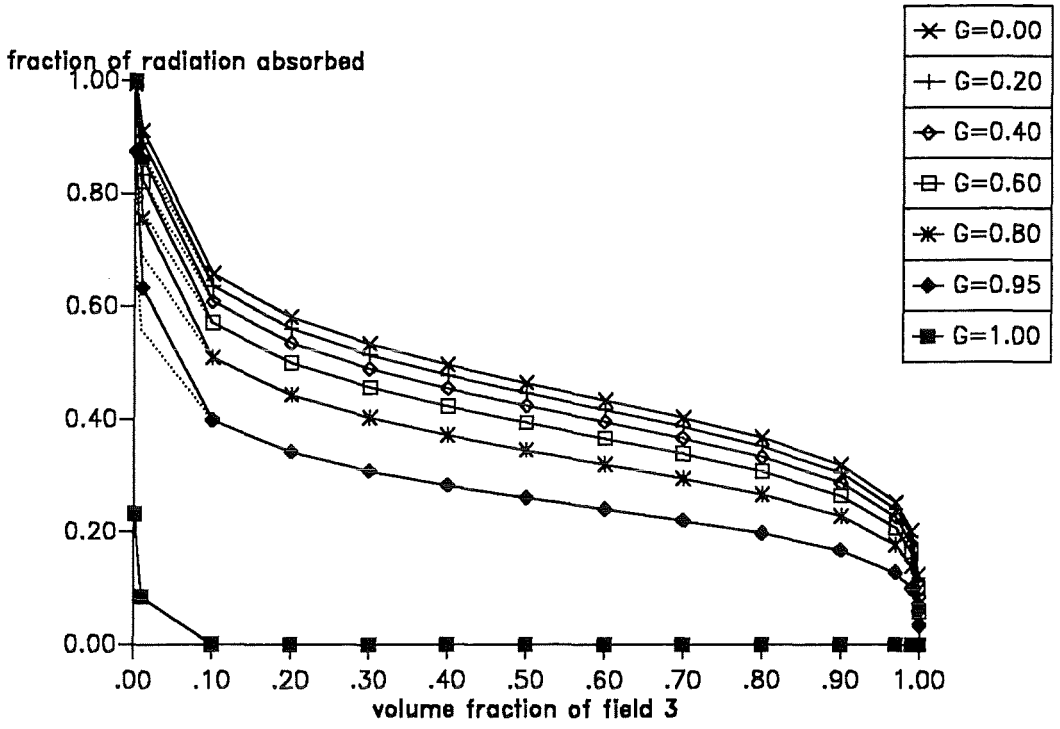


Fig. 12: As fig. 10 for a temperature of the radiant material of 3500 K.

Fig.s 13-15 are the same as fig.s 10-12 for a particle diameter of .0015 m, which is more typical for the conditions at the end of fragmentation. The absorption is somewhat smaller than that for the larger diameter, due to the smaller mean distances between field 3 surfaces, see section 2.3. The differences between fig.s 10-12 on the one hand and fig.s 13-15 are remarkably small, however.

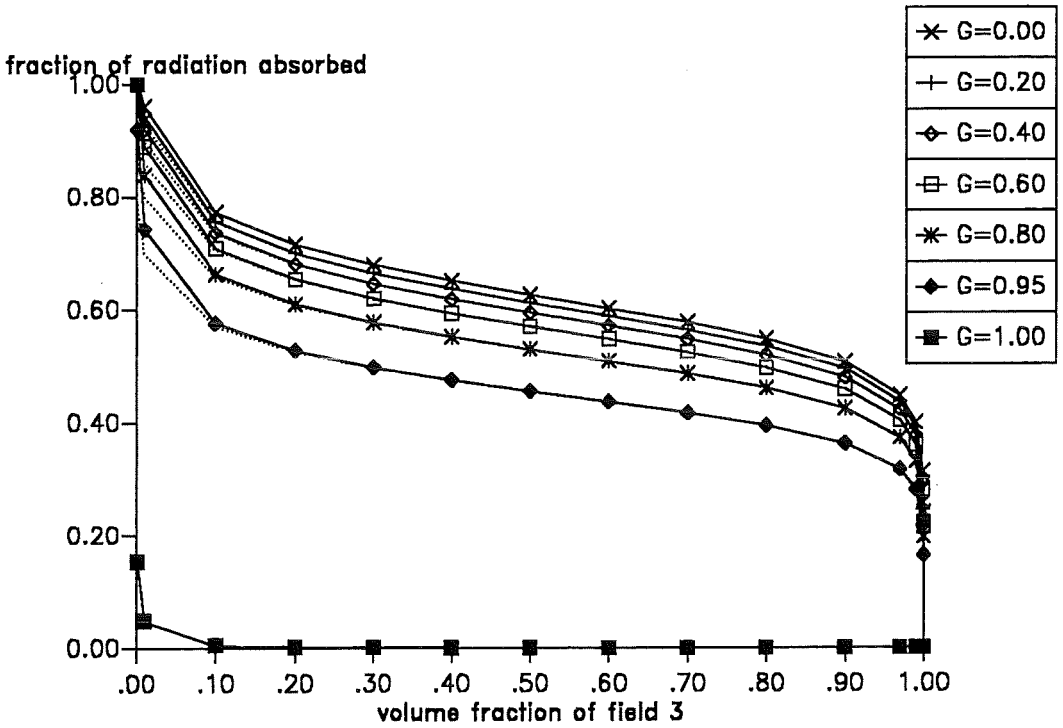


Fig. 13: Absorption of radiation. Temperature of the radiant material 2500 K, steam pressure .1 MPa, steam temperature 2000 K, particle diameter .0015 m (full lines: total absorption; dotted lines: absorption in water).

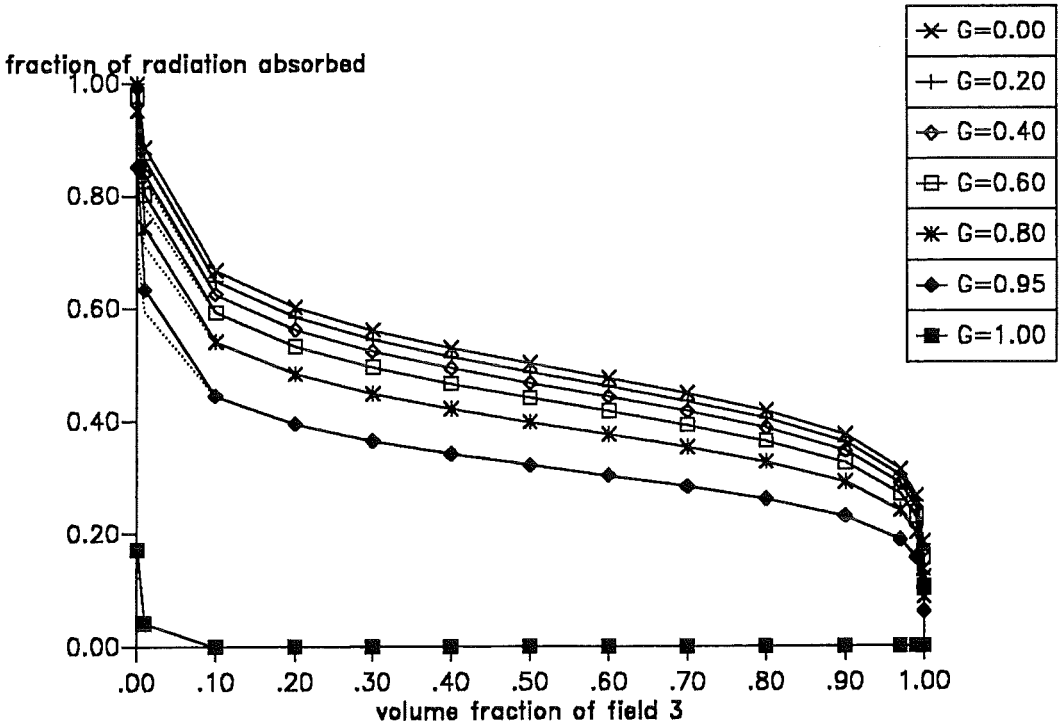


Fig. 14: As fig. 13 for a temperature of the radiant material of 3000 K.

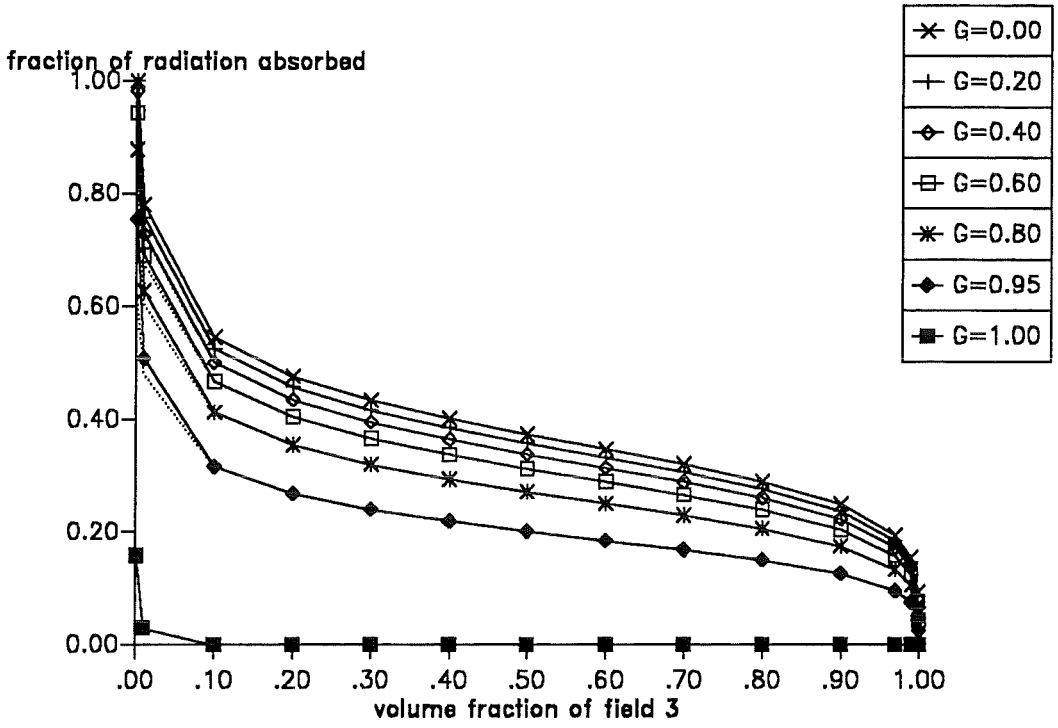


Fig. 15: As fig. 13 for a temperature of the radiant material of 3500 K.

Fig.s 16-18 are the same as fig.s 13-15 for steam at the saturation temperature of 373 K. The absorption in steam is a little more pronounced in this set of curves than in the foregoing one, as can be expected because of its larger density at the low temperature. The effect is not big, however: The maximum deviation of the total absorption shown in fig.s 13-15 from that in fig.s 16-18 is .02 in all cases involving water (it occurs, of course, for G = .95 at the lowest field 3 volume fractions), and .07 for the cases with pure steam. The probable reason is the resonance structure of the emissivity - and hence absorptivity - of steam with its much broader lines for higher steam temperatures, see fig. 8. The resultant more efficient absorption at high temperatures partly compensates for the lower steam density and the energy radiated back from the steam into field 3.

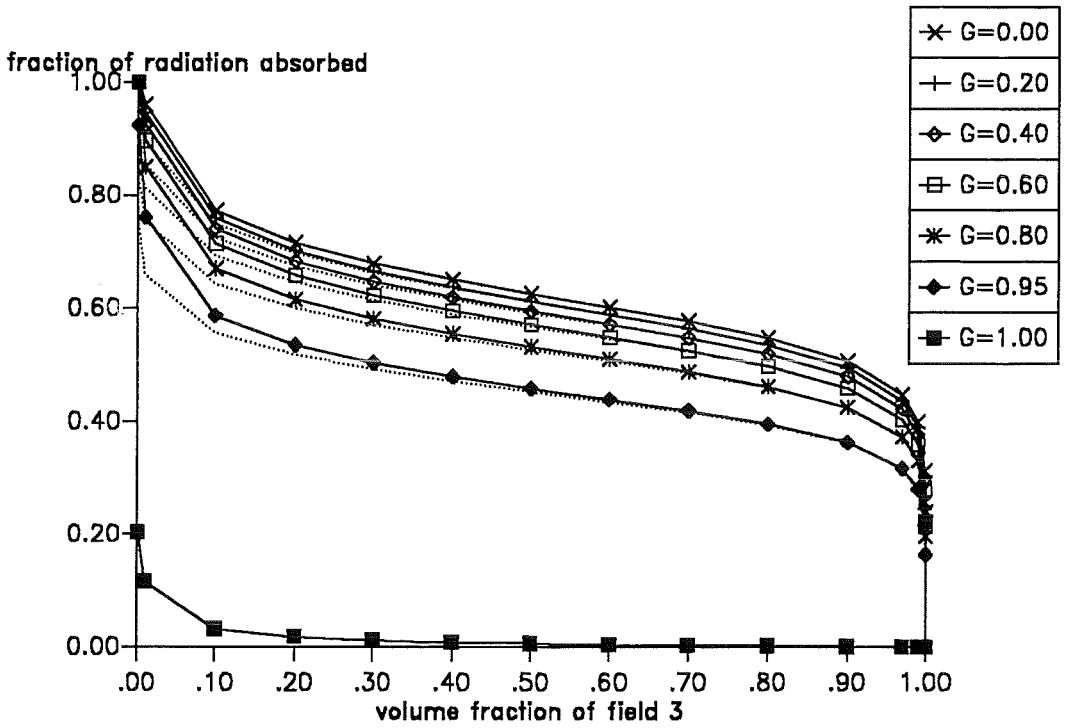


Fig. 16: Absorption of radiation. Temperature of the radiant material 2500 K, steam pressure .1 MPa, steam at saturation (373 K), particle diameter .0015 m (full lines: total absorption; dotted lines: absorption in water).

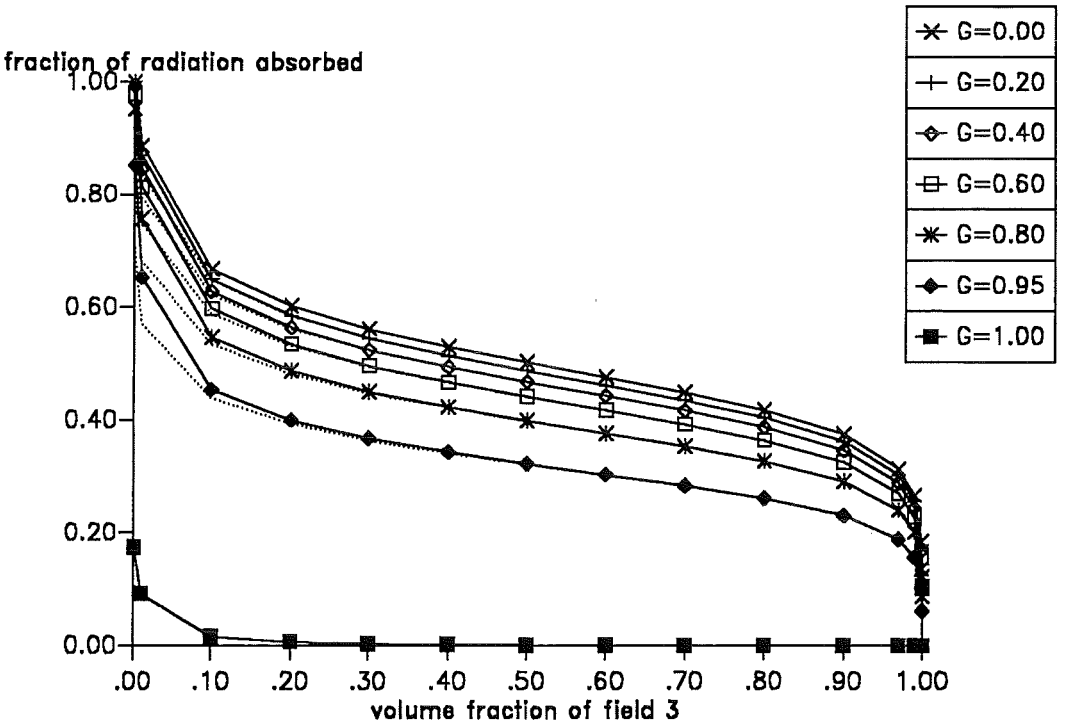


Fig. 17: As fig. 16 for a temperature of the radiant material of 3000 K.

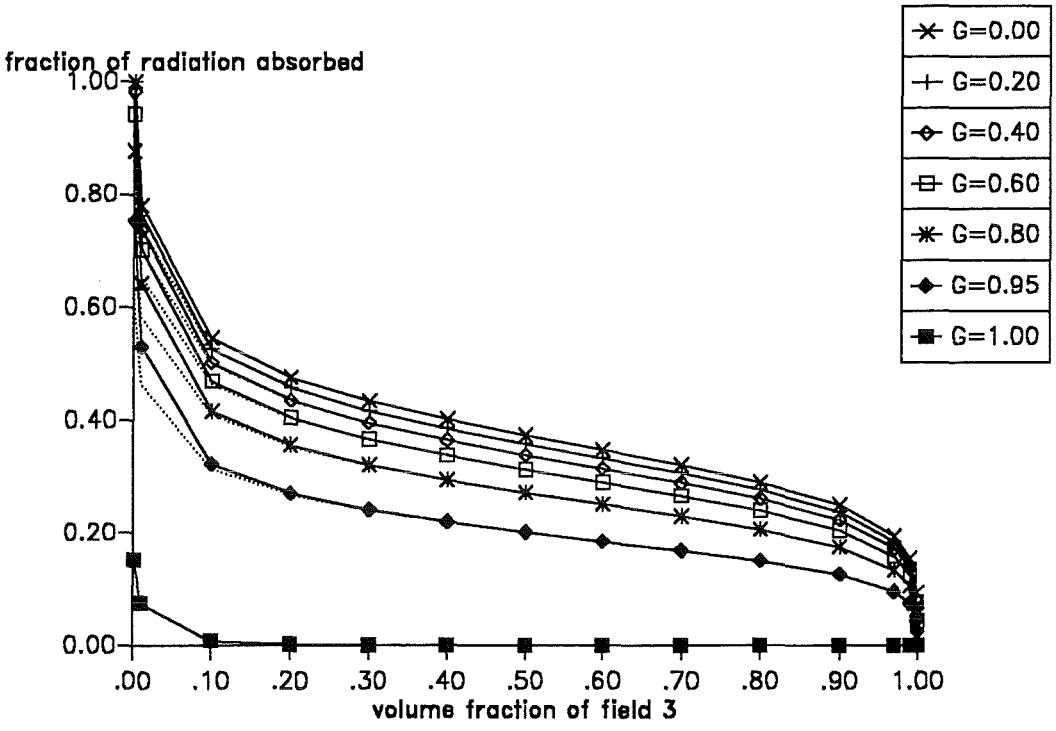


Fig. 18: As fig. 16 for a temperature of the radiant material of 3500 K.

Fig.s 19-21 are again the same as fig.s 13-15 for a steam pressure of 5 MPa (water temperature 537 K). The steam temperature is 2000 K. This set of figures demonstrates the importance of the absorption in steam at large steam pressures. The total absorption for cases involving water is at maximum .08 larger than the one for .1 MPa, with differences above .05 occuring for all $G \geq .4$ and up to rather large field 3 volume fractions. The absorption in pure steam grows by up to .38 (for $T_3 = 3500$ K and $\alpha_3 = .001$).

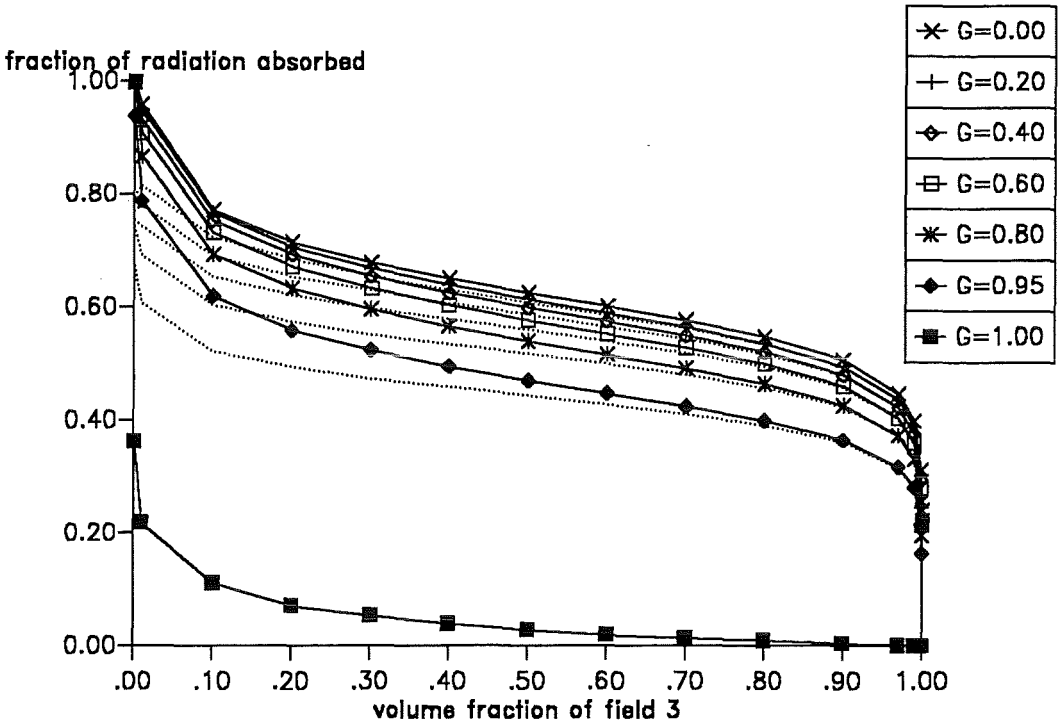


Fig. 19: Absorption of radiation. Temperature of the radiant material 2500 K, steam pressure 5 MPa, steam temperature 2000 K, particle diameter .0015 m (full lines: total absorption; dotted lines: absorption in water).

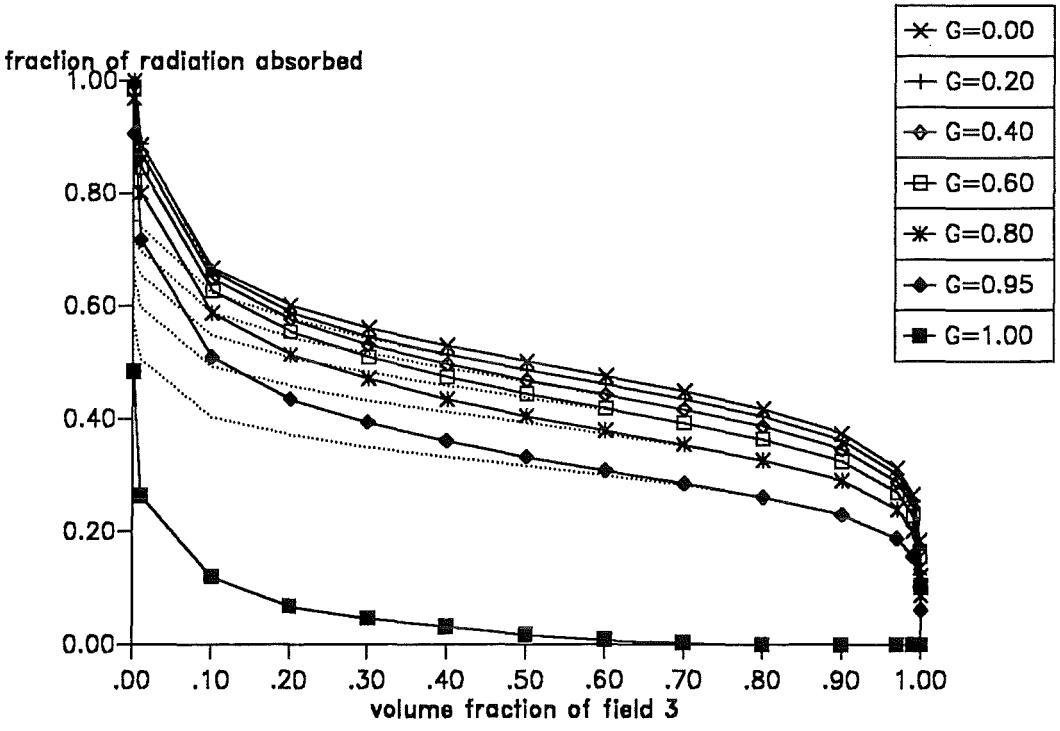


Fig. 20: As fig. 16 for a temperature of the radiant material of 3000 K.

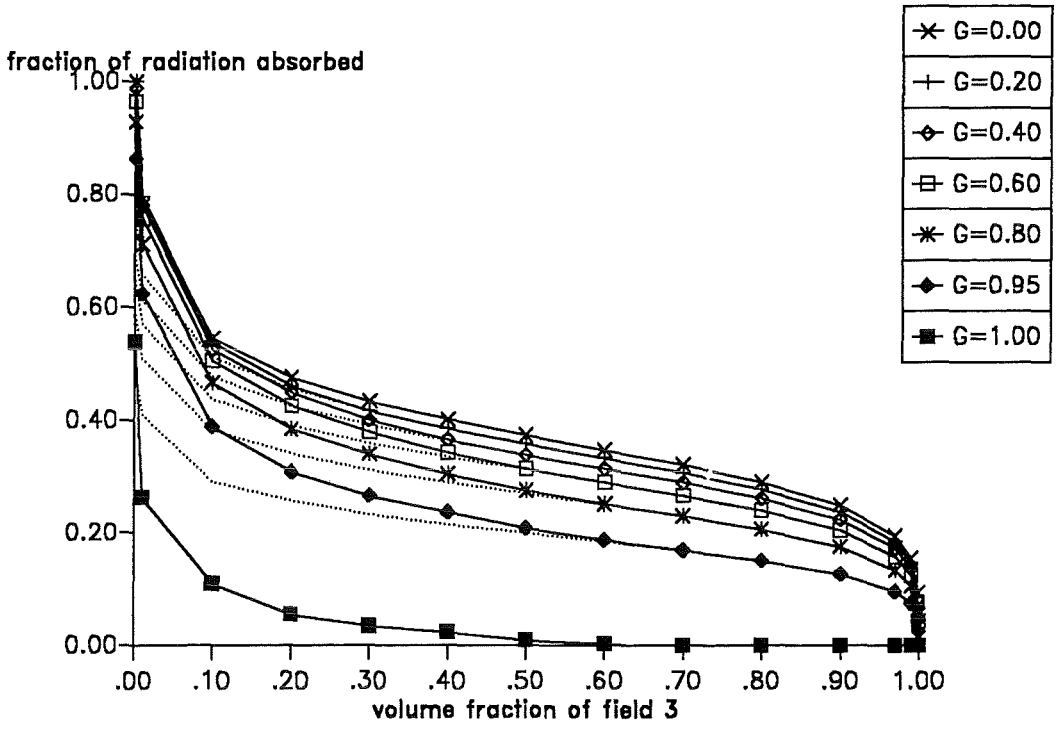


Fig. 21: As fig. 16 for a temperature of the radiant material of 3500 K.

4.2. Simple examples with 2x2 cells

The examples to be presented in this section are two-dimensional 2x2 cell cases with cell widths of 5 cm in both directions, cylindrical geometry and closed outer boundaries. The initial material distributions are homogeneous in the whole calculational domain and consist of steam, water and "corium", a mixture of uranium and zirconium oxide with a melt temperature of 2747 K. Common initial conditions of the cases are: A pressure of 2 MPa, water and steam temperatures of 484 K, 1.4 K below saturation, and a diameter of the corium particles of 5 cm. (The particle diameter has to be smaller than the cell dimensions in realistic calculations involving drag effects; here it serves only to define the heat transfer surface and can thus be chosen freely.) The cases differ in the initial temperature of the corium (below and above melting), and the initial volume fractions of the three fields (see table III). They have been chosen to cover a range of different situations in order to demonstrate the variability of the effects.

| Case | Volume Fractions of steam/water/corium | Corium temperature |
|---|---|---|
| A | 84.5/15.0/ 0.5 | 2700 |
| B | 84.5/15.0/ 0.5 | 2800 |
| C | 97.5/ 2.0/ 0.5 | 2800 |
| D | 54.5/45.0/ 0.5 | 2800 |
| E | 87.0/ 3.0/10.0 | 2700 |

**Table III:** Initial conditions of examples with 2x2 cells.

All calculations are terminated after 5 s problem time, and all except case E quickly reach the same material distribution with only steam in the two upper cells and practically identical conditions in the lower cells. The pressure rises homogeneously in the whole volume. Corium particle fragmentation happens as long as the initial corium temperature is above the melting temperature, i. e. only in cases B - D. Case E, the only one involving a higher corium volume fraction, exhibits a somewhat more dynamic behaviour: A longer time is needed for water and corium to settle in the lower zones, and a kind of sloshing movement takes place afterwards. This case displays already the interaction of the different models contained in the code, though still in a limited way.

Case A (fig. 22), with an initial corium temperature below melting, illustrates the basic effects of the model and the differences of the new and the old model. The initial pressure dip is due to a condensation of steam because of the initial subcooling. Subsequently the pressure rises slowly, because the heat transfer over the surface of the big solid particles that do not undergo fragmentation is limited. There is a very big difference between heat transfer with and without radiation, and also a marked difference between the old and the new model for radiative heat transfer. The radiative heat transfer to steam has no significant influence, whereas the transfer to water comprises about half of the total heat transferred, i. e. including heat transfer by convection.

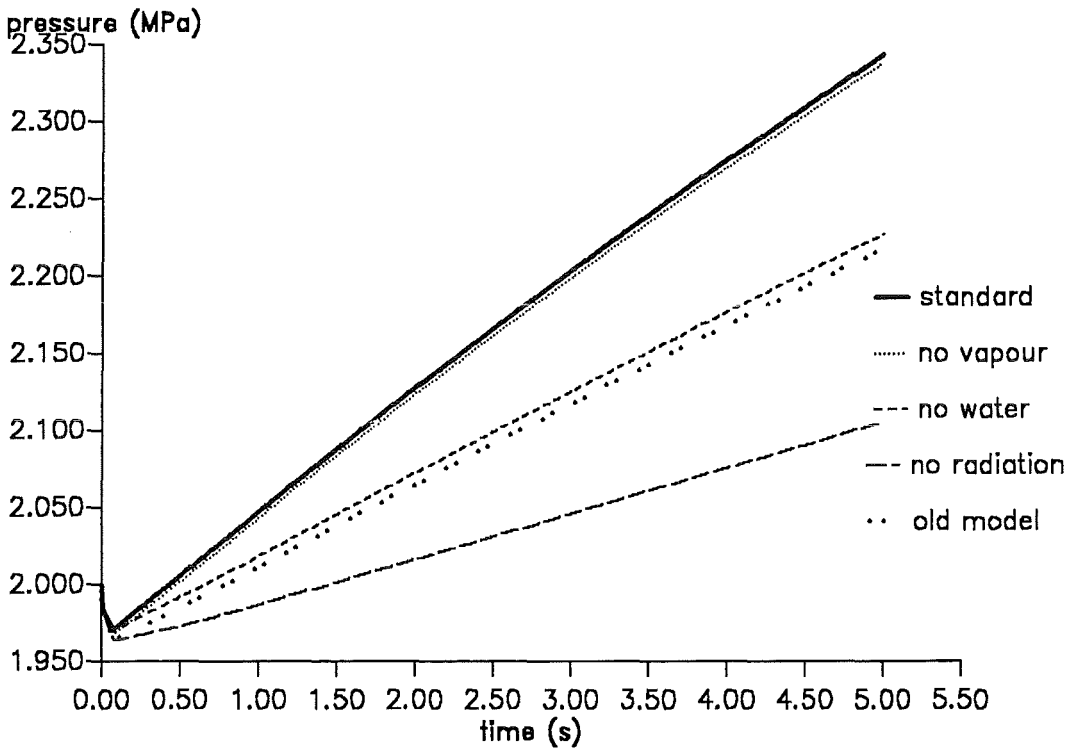


Fig. 22: Case A. Pressure vs. time for different models of radiative heat transfer. Initial melt temperature 2700 K, initial volume fraction of water 15%.

Case B is the same as case A for an initial temperature above melting (fig. 23). A fast fragmentation of the corium occurs in the beginning of the transient, leading to particle sizes of about .5 cm, that differ by no more than 1% for the different heat transfer models. The heat transfer is much faster because of the smaller particle sizes, the pressures reach much bigger values, and now a mitigating effect becomes evident: The temperatures remain higher for the cases with less efficient heat transfer models, as shown in fig. 24. Thus the temperature difference between melt and water, which drives the heat transfer, becomes bigger. This partly compensates for the less efficient radiative heat transfer, and the relative differences of the models become smaller in the long run. There remains, however, a marked difference among the times at which a given pressure is reached, as can be seen in fig. 23. The time for reaching 4 MPa, e. g., is nearly 40% bigger for the old model and 90% bigger for the model without any radiation, as compared to the standard model.

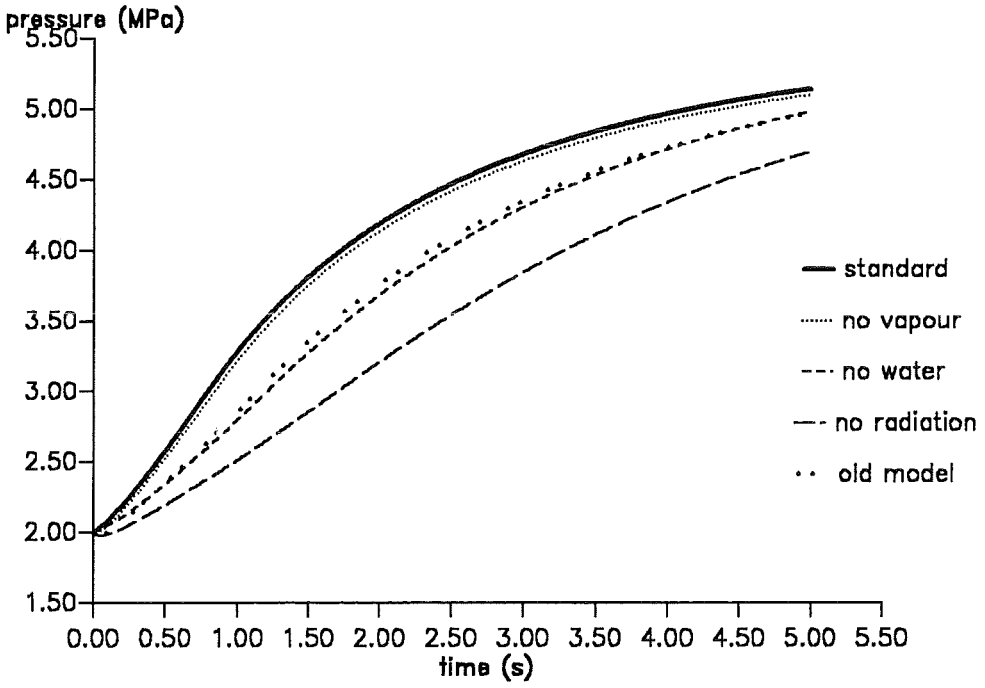


Fig. 23: Case B. Pressure vs. time for different models of radiative heat transfer. Initial melt temperature 2800 K, initial volume fraction of water 15%.

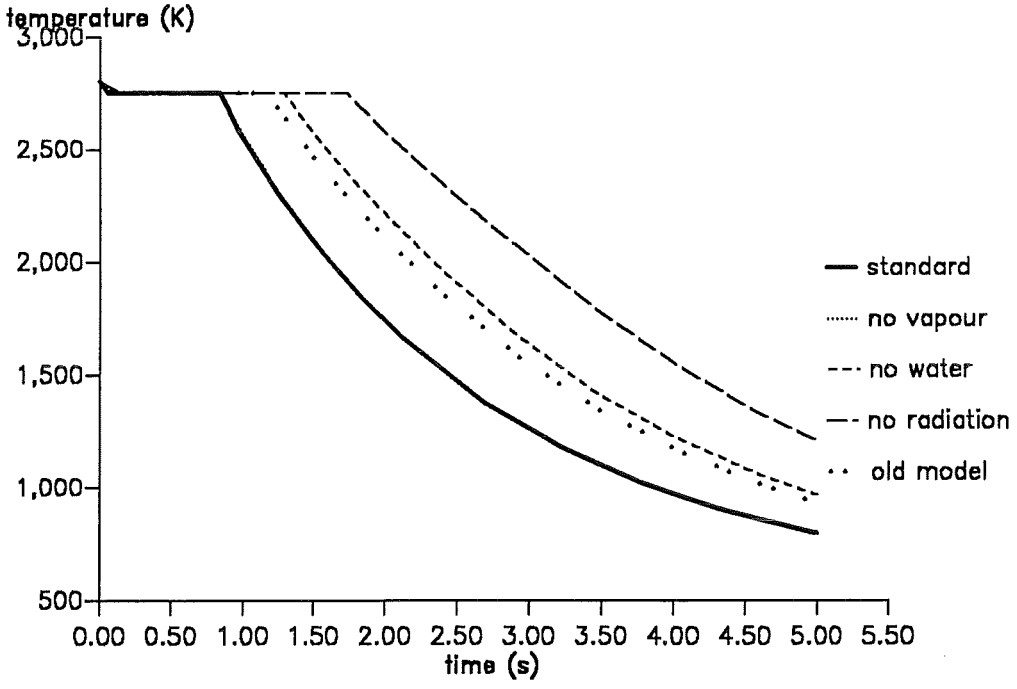


Fig. 24: Case B. Corium temperature vs. time for different models of radiative heat transfer.

Case C (fig. 25) starts with a smaller volume fraction of water and therefore shows a more pronounced influence of the radiative heat transfer to steam. There is again a fast fragmentation of the corium in the beginning of the transient, with particle sizes differing by no more than 1.5% for the different heat transfer models. The competitive absorption of radiation in water and in steam (see section 3.3) becomes evident in this case: The effect of totally suppressing the radiative heat transfer is much bigger than that of suppressing the absorption in only one of the two materials, because in the latter cases the second material can absorb a larger share of the total radiation. Case C demonstrates as well, how much the importance of radiative heat transfer depends on the individual conditions: Transfer by radiation clearly dominates in this case, and the older model is much less adequate than in cases A and B.

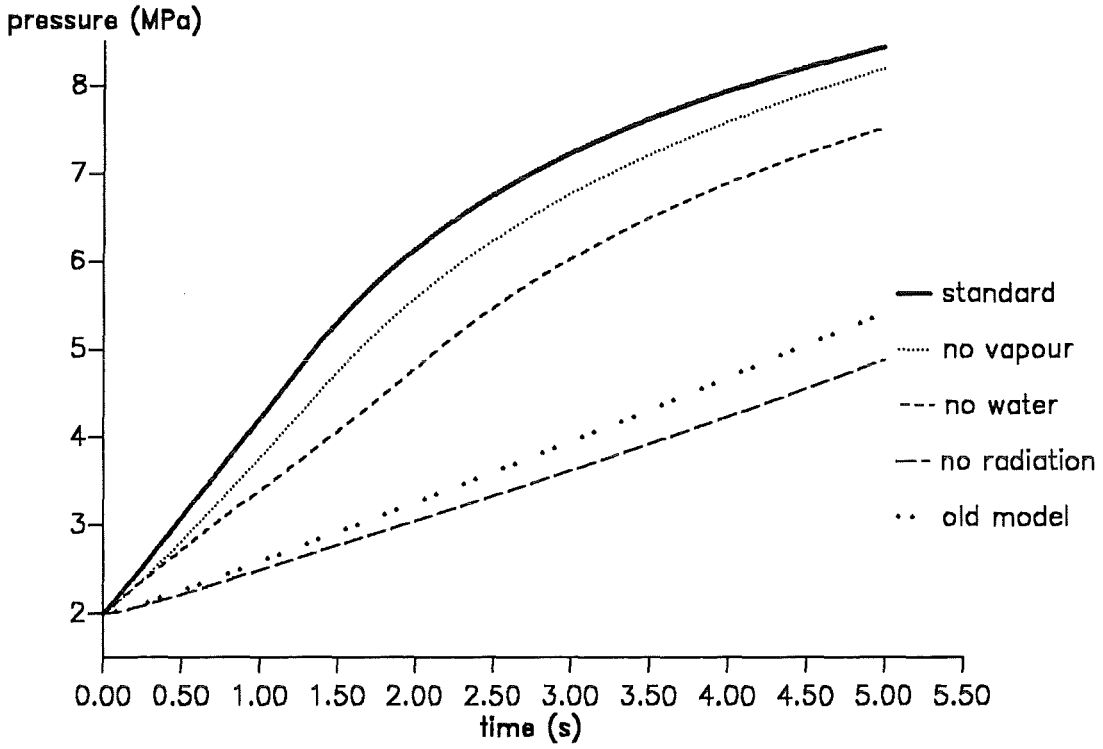


Fig. 25: Case C. Pressure vs. time for different models of radiative heat transfer. Initial melt temperature 2800 K, initial volume fraction of water 2%.

Case D (fig. 26) starts with a large volume fraction of water. The initial fragmentation leads to particle sizes differing by no more than .2%. The radiative heat transfer to steam has nearly no influence on the results in this case, as can be expected. The old model is practically identical to the new one. The radiative

heat transfer is of less importance compared to the convective heat transfer than in the foregoing cases.

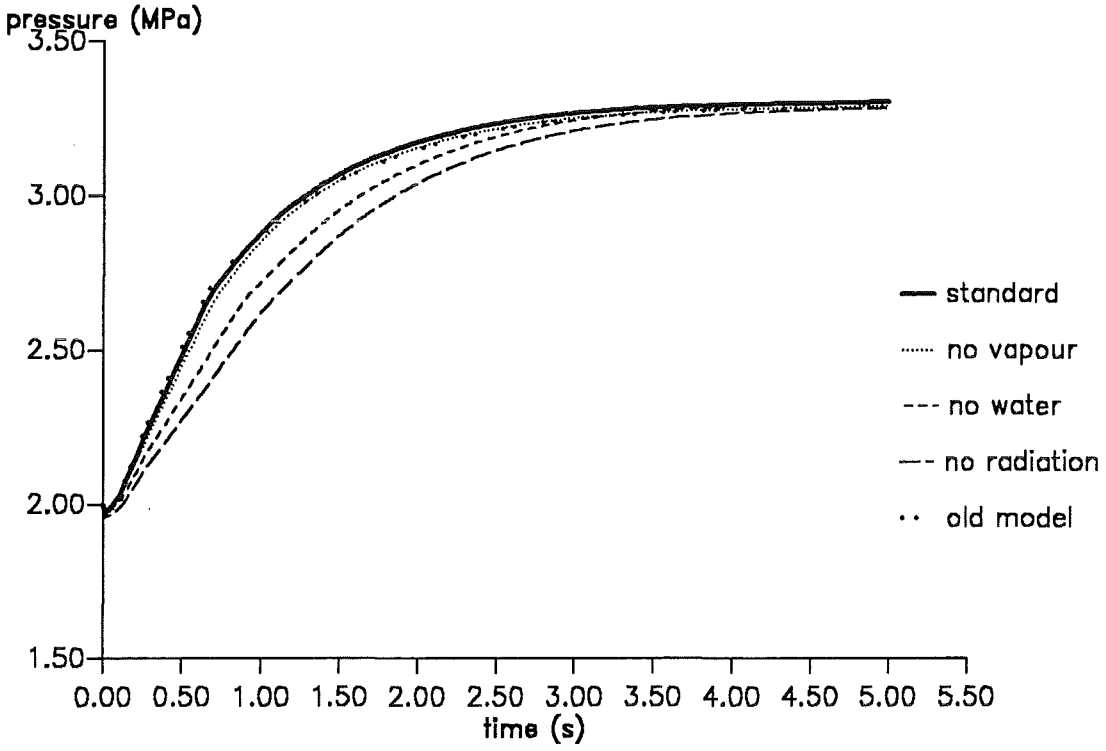


Fig. 26: Case D. Pressure vs. time for different models of radiative heat transfer. Initial melt temperature 2800 K, initial volume fraction of water 45%.

Case E (fig. 27) is the only one with a higher volume fraction of corium. The pressures rise to quite large values, as can be expected, though the corium temperature is below melting and thus no fragmentation occurs. The volume fraction of water is sufficiently small for total evaporation to occur with the more efficient heat transfer models. This happens at about 2.7 s for the standard model and the one without radiative heat transfer to vapour, and is evidenced by a change in the slope of the two curves. A very small water fraction remains in the mixture at 5 s when using the model without radiative heat transfer to water. There is a small irregularity in the pressure rise at about 1.2 s in this case, which is due to a spatial redistribution of steam. Another spatial movement, a sloshing of the corium in the two lower zones starting at about 3.5 s, causes the tapering off of the pressure rise at 4.7 s for the standard model. This case demonstrates, like case C, the inadequacy of the old model for small water fractions, and the large effect of the radiative heat transfer in such cases.

The results of the simple cases lead to the conclusion, that transient material behaviour can be expected to be decisively influenced by the radiative heat transfer to water at high temperatures of the melt. The heat transfer to water vapour has a smaller effect and is of importance mainly in situations with large volume fractions of steam.

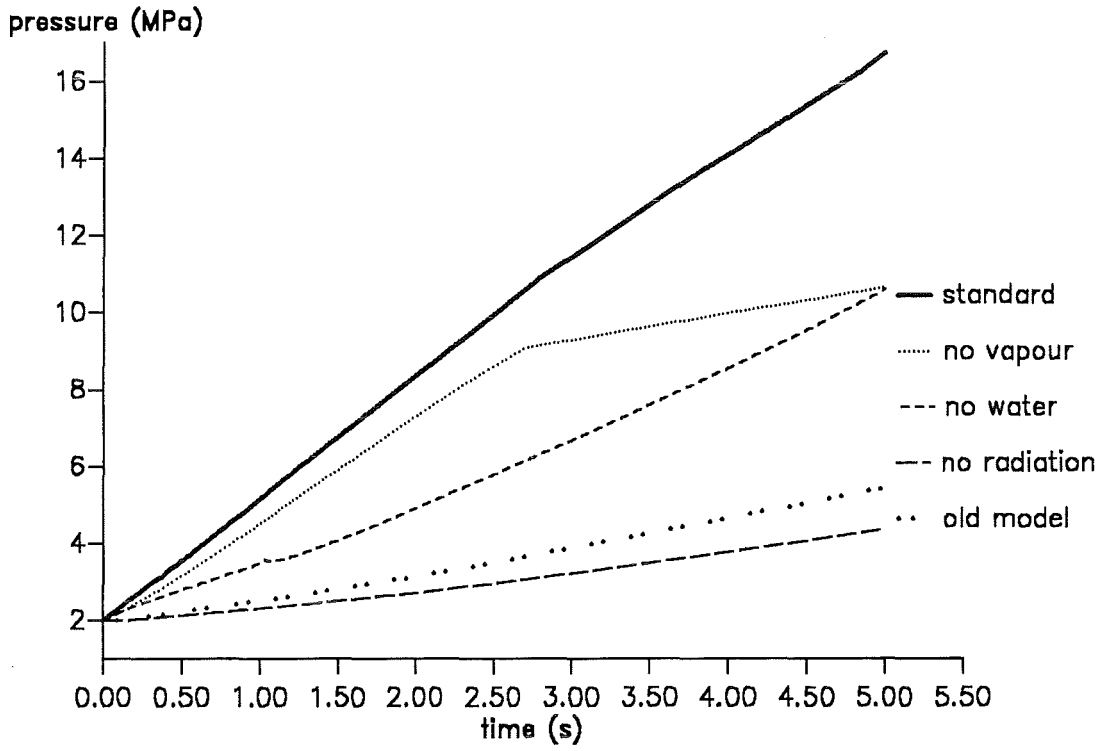


Fig. 27: Case E. Pressure vs. time for different models of radiative heat transfer. Initial melt temperature 2800 K, initial volume fraction of water 3%, of corium 10%.

## 4.3. Simulation of experiment FARO L-08

The second example is a simulation of FARO experiment L-08. This test is one of a series of experiments performed at JRC Ispra with the aim of investigating the quenching of molten core material in water. Details on the experiment can be found in ref. /10/. The test vessel is a container with a radius of 35.5 cm and a height of about 3 m, filled with water at saturation temperature up to a height of 1 m; the initial pressure in the container is 5.8 MPa. 44 kg of a molten mixture of uranium and zirconium oxide at 3000 K are dropped from an intermediate melt catcher at a height of 1.53 m above the surface of the water. The representation

of this geometry used in the simulation with IVA-KA is shown in fig. 28; it is two-dimensional and cylindrical as in the simple examples.

Fig. 29 shows a comparison of the time dependent pressures in the gas dome, resulting from the calculations with the same five different models for radiative heat transfer as in section 4.2. The measured results are added for the sake of completeness, but the geometric representation chosen for this study is somewhat too coarse to allow for a serious comparison.

Some of the results shown in fig. 29 are quite unexpected. The old model and the models without radiative heat transfer to water resp. vapour yield smaller pressures than the new model, as expected. Quite surprisingly, however, the model without any radiation yields the highest pressures of all simulations beyond 1.0 s. The reason for this is revealed in fig. 30, which shows the diameters of the corium particles after the corium temperatures have dropped below the liquidus, i. e. when fragmentation has stopped. The diameters are about 30% smaller in the "no radiation" case, leading to a 30% bigger corium surface and thus a much more efficient heat transfer. This effect is due to the initially less efficient heat transfer, which causes a longer time at temperatures above the liquidus, and thus longer fragmentation.

Fig.s 29 and 30 show, too, that the old model yields equally small corium particle diameters (for the same reason as the "no radiation" case), and yet results in much smaller pressures. The old model is thus less efficient than is evident from the pressures, since part of its inefficiency is compensated by the larger corium surface reached.

The pressure yields of the models without radiative heat transfer to water resp. steam are less spectacular but also unexpected. According to the simple cases, one would expect the pressures to be higher for the model without radiative heat transfer to steam. Inspection of fig. 30 shows slighly smaller corium diameters for the less efficient heat transfer model (the one without radiative heat transfer to water), i. e. the same compensating effect as in the case of the model without radiation seems to be active.

The main conclusion from all calculations is thus, that compensating effects, e. g. fragmentation, may limit the effect of the new model, when used in the framework of a full multiphase, multicomponent code. It can be expected, however, to yield somewhat higher pressures for quenching situations than the older model contained in IVA3.

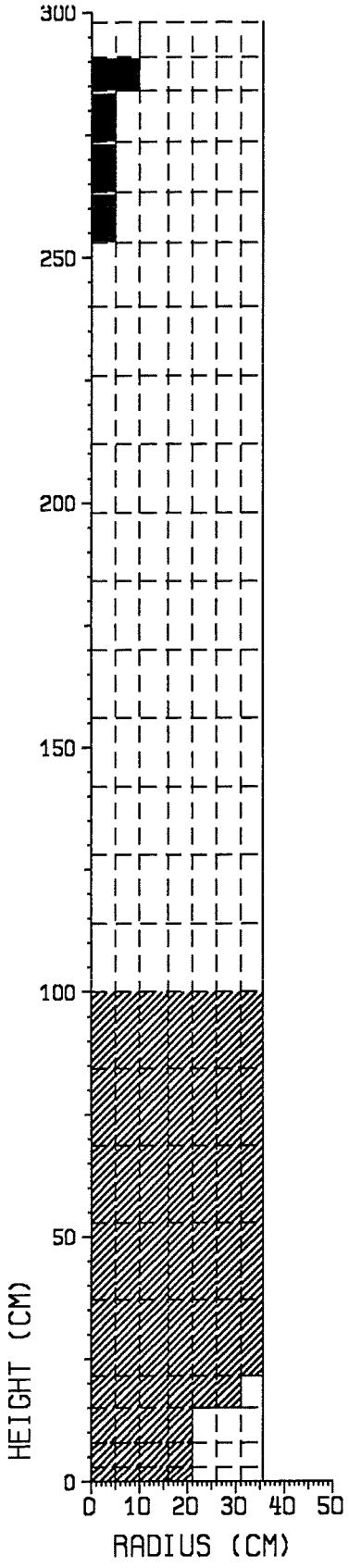


Fig. 28: Initial configuration of FARO L-08. Black areas: melt; shaded areas: water; white areas: gas. The volume fractions in each cell are represented as area fractions.

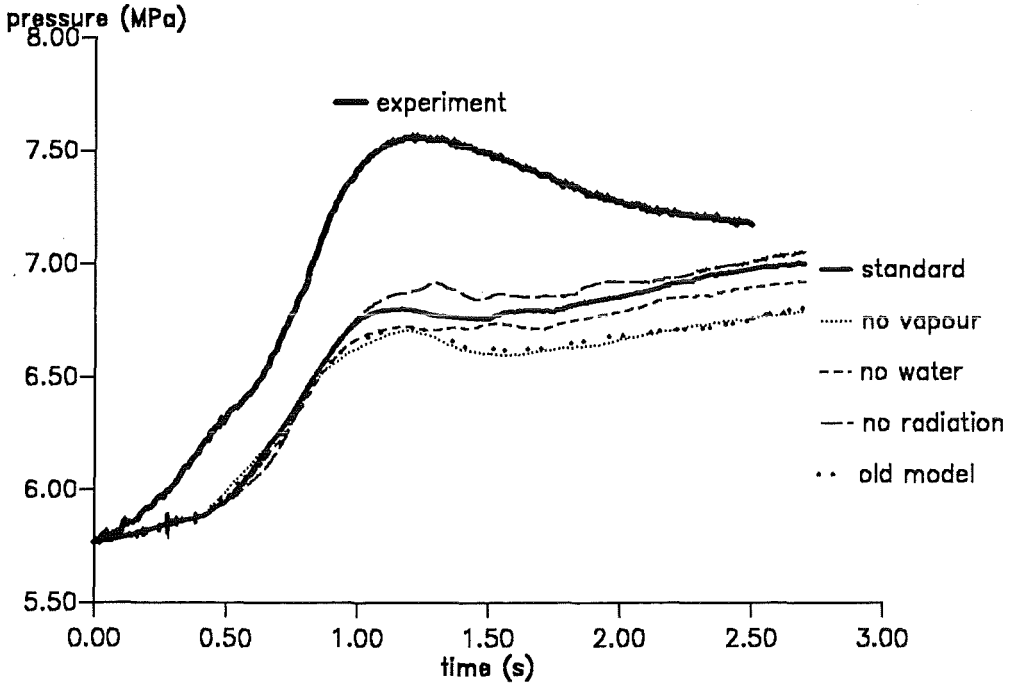


Fig. 29: Time dependent pressure rise in a simulation of FARO experiment L-08.

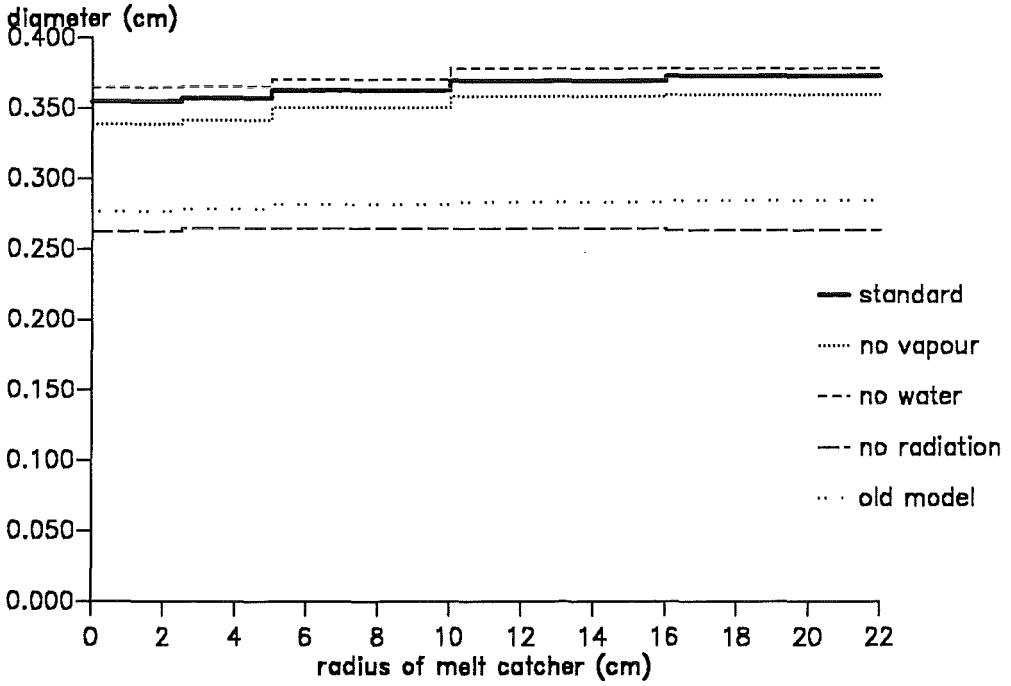


Fig. 30: Corium particle diameter vs. radius, at the bottom of the test vessel, at time 2.7 s. Simulation of FARO experiment L-08.

## 5. CONCLUSIONS

A more realistic model for radiative heat transfer, to be used in multiphase, multicomponent programmes, was developed and tested in the framework of the IVA-KA code. The transport of radiation across the calculational mesh, i. e. over long distances is not covered by the model. For quenching situations, the new model can be expected to yield higher pressures than the old model contained in IVA3. Transients involving water vapour at high densities can be modelled more adequately.

Acknowledgement:

The author wishes to gratefully acknowledge many helpful and valuable discussions with H. Jacobs. The study by Mme. Battail and M. Berthoud /11/ served as a very useful introduction to the problems.

**Table of symbols:**

| | |
|---|---|
| $A_v$ | fraction of energy absorbed in water vapour |
| $A_w$ | fraction of energy absorbed in water |
| $A_1$ | fraction of energy absorbed by a water layer of thickness 1 mm |
| $A_{30}$ | same as $A_1$ for thickness 30 mm |
| $A_{10}(S)$ | function describing the absorptivity of water at 1000 K |
| $A_{25}(S)$ | same as $A_{10}(S)$ for 2500 K |
| $A_{35}(S)$ | same as $A_{10}(S)$ for 3500 K |
| $D_c$ | diameter of equivalent cell around melt particle |
| $D_i$ | diameter pertaining to field i (e. g. of bubbles, droplets...) |
| $F_{surf}$ | fraction of the energy absorbed in water which is deposited in its surface |
| O | surface of the melt |
| Q | radiative energy emitted by the melt |
| $dQ_v$ | radiative heat transferred to the water vapour |
| $dQ_w$ | radiative heat transferred to the water |
| S | thickness of water layer |
| $\overline{S}$ | mean distance for radiation from emission to reabsorption in field 3 |
| $T_i$ | temperature of field i |
| y | product of vapour pressure and thickness of air/vapour mixture |
| $\alpha_i$ | volume fraction of field i |
| $\varepsilon_v$ | emissivity of water vapour |
| $\varepsilon_3$ | emissivity of the melt (.7) |
| $\lambda$ | wavelength |
| $\sigma$ | Stefan-Boltzmann constant |

**References:**


/1/ H. Jacobs, M. Lummer, B. Stehle, K. Thurnay, L. Väth: IVA-KA, a Three-Field Model of Premixing in Steam Explosions. Transactions of the ENC '94 International Nuclear Congress, Lyon, 2. - 6. 10. 1994, Vol. II, p. 542

/2/ N. I. Kolev: The code IVA3 for modelling of transient three-phase flows in complicated geometry. Kerntechnik 59 (1993) 147

/3/ N. I. Kolev: IVA3: Computer Code for Modelling of Transient Three Dimensional Three Phase Flow in Complicated Geometry. Program Documentation: Input Description. Kernforschungzentrum Karlsruhe, Report Nr. KfK 4950 (1991)

/4/ D. F. Fletcher: Assessment and Development of the Bankoff and Han Coarse Mixing Model. UKAE Culham Laboratory, Report Nr. CLM-R252 (1985)

/5/ R. V. Meghreblian, D. K. Holmes: Reactor analysis. McGraw-Hill, New York, 1960, p. 628.

/6/ J. B. Knowles: A Mathematical Model of Vapour Film Destabilisation. AEE Winfrith, Report Nr. AEEW-R 1937 (1985)

/7/ H. C. Hottel, A. F. Sarofim: Radiative Transfer. McGraw-Hill, New York, 1967

/8/ P. Docherty: Prediction of Gas Emissivity for a Wide Range of Process Conditions. Proceedings of the 7th Heat Transfer Conference, Munich, 6.-10. 9. 1982 (Hemisphere Publ. Corp., Wash.) Vol. 2, p. 481

/9/ F. R. Steward, Y. S. Kocaefe: Total Emissivity and Absorptivity for Carbon Dioxide, Water Vapor and Their Mixtures. Proceedings of the 8th Heat Transfer Conference, San Francisco, 17.-22. 8. 1986 (Springer, Berlin) Vol. 2, p. 735

/10/ D. Magallon, H. Hohmann: High Pressure Corium Melt Quenching Tests in FARO. Nucl. Eng. Des. 155 (1995) 253

/11/ S. Battail, G. Berthoud: Etude du transfert radiatif dans les phénomènes d'interaction corium-eau. Private communication, 1993